Article

Cell Reports

Combinatorial Pharyngeal Taste Coding for Feeding Avoidance in Adult *Drosophila*

Graphical Abstract

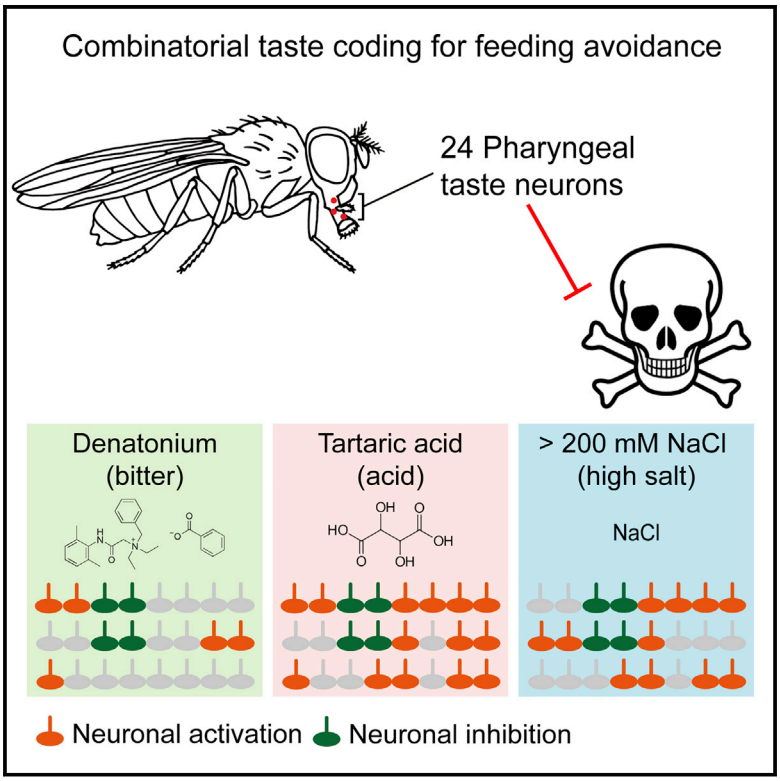

Authors

Yu-Chieh David Chen, Scarlet Jinhong Park, Ryan Matthew Joseph, William W. Ja, Anupama Arun Dahanukar

Correspondence

anupama.dahanukar@ucr.edu

In Brief

Chen et al. perform functional and behavioral experiments to study the roles of different subsets of pharyngeal neurons in governing food avoidance in flies. They find evidence that rejection of different categories of aversive compounds is dependent on distinct combinations of pharyngeal taste neurons.

Highlights

- Flies with only pharyngeal taste input avoid many aversive compounds
- Activation of single aversive pharyngeal neurons suppresses food intake
- Distinct subsets of pharyngeal neurons drive avoidance of different tastants
- Second-order neurons in pharyngeal circuits project to two main brain regions

Chen et al., 2019, Cell Reports *29*, 961–973
October 22, 2019
https://doi.org/10.1016/j.celrep.2019.09.036

CellPress

Cell Reports
Article

Combinatorial Pharyngeal Taste Coding for Feeding Avoidance in Adult *Drosophila*

Yu-Chieh David Chen,[1] Scarlet Jinhong Park,[2,3] Ryan Matthew Joseph,[4] William W. Ja,[2,3] and Anupama Arun Dahanukar[1,4,5,*]
[1]Interdepartmental Neuroscience Program, University of California, Riverside, CA 92521, USA
[2]Department of Neuroscience, The Scripps Research Institute, Jupiter, FL 33458, USA
[3]Skaggs Graduate School, The Scripps Research Institute, Jupiter, FL 33458, USA
[4]Department of Molecular, Cell and Systems Biology, University of California, Riverside, CA 92521, USA
[5]Lead Contact
*Correspondence: anupama.dahanukar@ucr.edu
https://doi.org/10.1016/j.celrep.2019.09.036

SUMMARY

Taste drives appropriate food preference and intake. In *Drosophila*, taste neurons are housed in both external and internal organs, but the latter have been relatively underexplored. Here, we report that *Poxn* mutants with a minimal taste system of pharyngeal neurons can avoid many aversive tastants, including bitter compounds, acid, and salt, suggesting that pharyngeal taste is sufficient for rejecting intake of aversive compounds. Optogenetic activation of selected pharyngeal bitter neurons during feeding events elicits changes in feeding parameters that can suppress intake. Functional dissection experiments indicate that multiple classes of pharyngeal neurons are involved in achieving behavioral avoidance, by virtue of being inhibited or activated by aversive tastants. Tracing second-order pharyngeal circuits reveals two main relay centers for processing pharyngeal taste inputs. Together, our results suggest that the pharynx can control the ingestion of harmful compounds by integrating taste input from different classes of pharyngeal neurons.

INTRODUCTION

Insects perceive environmental stimuli through sensory systems and use this information to guide behavioral responses. In some instances, a sensory system encompasses multiple organs, which are thought to have specialized contributions to behavior. In the gustatory system of a well-established genetic model, *Drosophila melanogaster*, there are multiple taste organs, present externally throughout the body (labellum, legs, and wing margins) and internally in pharyngeal organs (Freeman and Dahanukar, 2015; Joseph and Carlson, 2015). Although the labellum and legs may be important for the initial assessment of quality due to their first contact with food, pharyngeal taste organs are believed to monitor food quality during ingestion. However, the specific role of pharyngeal taste in controlling feeding has not been explored in depth.

Presumably, pharyngeal taste organs could serve as a final checkpoint to monitor food quality. Pharyngeal taste input is anatomically represented in regions of the CNS that are distinct from other taste organs (Kwon et al., 2014; Wang et al., 2004), which is consistent with potentially separable location-dependent roles of taste input. This notion is supported by recent studies showing that pharyngeal gustatory receptor neurons (GRNs) elicit behavioral responses to appetitive tastants that are distinguishable from those elicited by external GRNs. External GRNs contribute to the initiation of feeding and trigger the proboscis extension reflex (PER), an indication of acceptance behavior, whereas those in the pharynx sustain feeding bouts (LeDue et al., 2015). Similarly, external GRNs initiate PER to yeast, but those housed in taste pegs lining the inner surface of labellum sustain feeding (Steck et al., 2018). Pharyngeal GRNs have also been shown to mediate the rejection of some compounds (Soldano et al., 2016; Kang et al., 2010), but the extent to which the pharynx controls feeding avoidance is not clear.

Recently, we created receptor-to-neuron maps of pharyngeal taste organs, which revealed the presence of multiple classes of taste neurons (Chen and Dahanukar, 2017), consistent with the idea that the pharynx may independently assess food quality. To investigate how pharyngeal taste input affects feeding behaviors, we took advantage of *Pox-neuro* (*Poxn*) mutants, in which all external taste bristles are transformed into mechanosensory bristles (Awasaki and Kimura, 1997; Nottebohm et al., 1992) but all pharyngeal taste neurons are retained (Chen and Dahanukar, 2017; Chen et al., 2018). We first characterized feeding preference and food intake of *Poxn* mutants and found that behavioral avoidance of a diverse panel of bitter compounds, high concentrations of salt, and tartaric acid is similar to that of control flies. Notably, we found a strong correlation between *Poxn* and control flies in feeding aversion intensity and food intake suppression, implicating sufficiency of pharyngeal taste for feeding control. Optogenetic activation of two different pharyngeal bitter neurons only during the feeding events, in otherwise wild-type flies, either reduced meal size or increased the time to the next meal, supporting the notion that some pharyngeal GRNs play a role as gatekeepers to manage food entry into the digestive tract by suppressing food intake. To further investigate the neuronal basis of feeding avoidance by pharyngeal taste, we used a genetic dissection strategy to silence different classes of

pharyngeal GRNs and found that feeding aversion could be achieved by multiple subsets of pharyngeal GRNs. *Ex vivo* calcium imaging data showed that denatonium, tartaric acid, and high salt inhibited the sucrose-evoked activity of pharyngeal *Gr43a* sweet GRNs. This inhibition is not a general feature for sugar-sensing pharyngeal GRNs because denatonium activated rather than inhibited *Ir60b* pharyngeal GRNs, consistent with their role in limiting consumption. Furthermore, feeding avoidance of denatonium, tartaric acid, or high salt was eliminated only when both inhibition of pharyngeal *Gr43a* sweet GRNs and activation of different combinations of aversive pharyngeal GRNs were absent. Tracing pharyngeal second-order circuits revealed that both appetitive and aversive pharyngeal GRNs conveyed inputs to two common brain areas (pars intercerebralis and lateral protocerebrum), suggesting that pharyngeal taste is represented across brain regions. Our study demonstrates an important role of pharyngeal taste in controlling food choice and intake and provides a foundation for further functional investigation of higher-order taste circuits.

RESULTS

Poxn Mutants Respond to a Broad Range of Bitter Compounds

Previous studies have used *Poxn* mutants to understand the role of pharyngeal sweet GRNs, which promote sugar consumption and local search behaviors (Murata et al., 2017; LeDue et al., 2015). To evaluate the role of the pharynx in feeding avoidance, we also took advantage of *Poxn* mutants, which serve as a good model for dissecting the function of pharyngeal taste without other confounding taste inputs (Chen et al., 2018). Specifically, we characterized feeding preferences of *Poxn* mutants in binary choice assays for various categories of aversive tastants, including high concentrations of tartaric acid and salt (Zhang et al., 2013; Charlu et al., 2013), as well as compounds perceived as bitter by humans and avoided by flies (Weiss et al., 2011). All aversive tastants were tested in mixtures with sucrose against sucrose alone, a context in which the reduction in the appetitive value of the mixture compared to that of sucrose alone can be gauged. *Poxn* flies rejected sucrose mixtures containing tartaric acid (Figure 1A), or salt at concentrations of 200 mM and above (Figure 1B), displaying food preferences similar to those of control flies. By contrast, we observed some variation in behavioral responses to bitter compounds between control and *Poxn* mutant flies. Nine bitter compounds were selected on the basis of their ability to elicit different degrees of avoidance in previously reported binary choice assays (Weiss et al., 2011). We tested each compound across a range of concentrations and measured slopes for trend lines derived from linear regression analyses for each concentration curve for control and *Poxn* flies. Based on the results, bitter tastants could be broadly separated into two categories depending on the degree to which *Poxn* mutants showed behavioral sensitivity to them. Denatonium, lobeline, quinine, papaverine, and coumarin elicited similar degrees of feeding avoidance in *Poxn* mutants and control flies, although the mutants showed reduced feeding avoidance for some of these compounds at higher concentrations (Figure 1C). The slopes of trend lines for these compounds, referred to as pharynx sensitive, ranged from −0.43 to −0.77 for both genotypes. However, *Poxn* mutants showed little or no feeding aversion to caffeine, theophylline, N,N-diethyl-meta-toluamide (DEET), and strychnine, all of which induced strong concentration-dependent behavioral avoidance in control flies (Figure 1D). For these compounds, referred to as pharynx insensitive, the slopes of trend lines ranged from −0.40 to −0.78 in control flies but −0.11 to −0.22 in the *Poxn* mutants.

Pharyngeal Taste Controls the Intensity of Feeding Aversion

To better compare behavioral responses to bitter compounds in control and *Poxn* flies, we first extrapolated an iso-attractive concentration for each compound, [IA], a concentration that rendered a mixture with 5 mM sucrose equally as palatable as 1 mM sucrose alone (preference index = 0 in binary choice assay), based on the linear regression analyses. Thus, a low [IA] value indicates strong aversion and a high [IA] value indicates weak aversion (Figure 1E). We calculated [IA] values for most compounds for both control and *Poxn* flies, except DEET and strychnine, as *Poxn* mutants did not show concentration-dependent behavioral responses to these compounds. The compounds could be clustered based on the differences in the [IA] between the controls and the mutants. (Figure 1E). Control flies generally rejected pharynx-sensitive compounds (e.g., denatonium, lobeline, quinine, papaverine, and coumarin) to a greater extent than those categorized as pharynx insensitive (e.g., caffeine and theophylline) (Figure 1E). Surprisingly, we found that the order of aversiveness of the tastants was similar between the control and the mutant flies, and there was a strong positive correlation between the [IA] values from *Poxn* mutants and those from control flies ($R^2 = 0.9617$, $p < 0.0001$) (Figure 1F). The similarity in patterns of feeding aversion between *Poxn* and control flies suggests that pharyngeal taste alone can be sufficient for determining overall feeding avoidance of a variety of bitter compounds.

Pharyngeal Taste Controls the Suppression of Food Intake

Aversive effects of bitter compounds can be observed not only in feeding preference assays but also in suppression of food intake (Weiss et al., 2011; Sellier et al., 2011). Therefore, we next investigated the role of pharyngeal taste in determining ingestion suppression of aversive tastants. We used a newly developed Activity Recording Capillary Feeder (ARC) assay in which food intake, meal size, and meal frequency can be measured in individual flies (Murphy et al., 2017). We compared consumption of 100 mM sucrose alone or in mixtures with eight different bitter compounds by control and *Poxn* mutant flies for 24 h. In control flies, we found that different bitter compounds suppressed food intake to varying degrees. Denatonium, lobeline, strychnine, and quinine evoked strong feeding suppression, whereas papaverine, coumarin, caffeine, and theophylline did so to a weaker extent (Figure 2A). We noticed that the aversiveness ranking of bitter compounds in the short-term feeding choice assay (Figure 1E) was distinct from the ability of bitter compounds to suppress food intake in a 24-h food consumption assay (Figure 2A). However, the food intake of all tested diets was not significantly

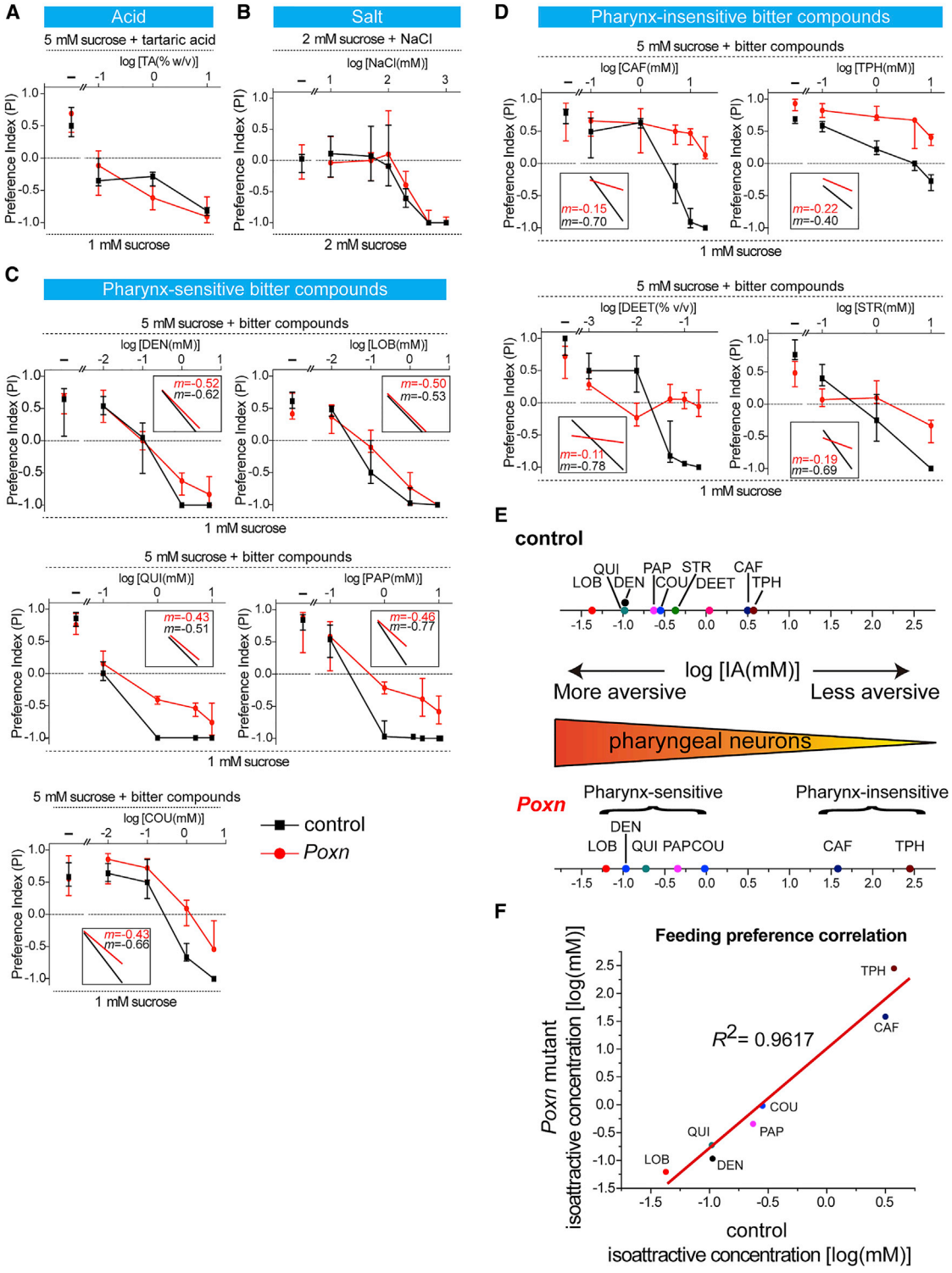

Figure 1. *Pox neuro* (*Poxn*) Flies Display Feeding Avoidance of Aversive Tastants

(A–D) Results of binary feeding choice assays with sucrose alone tested against mixtures of sucrose tartaric acid (A), salt (B), "pharynx-sensitive" bitter compounds (C), and "pharynx-insensitive" bitter compounds (D); concentrations for all tastants as indicated. The dotted lines at PI = 0 indicate an equal preference for the two choices. Insets in (C) and (D) show trend lines and slopes derived from linear regression analysis. Genotypes were control (w^{1118}) and *Poxn* ($Poxn^{\Delta M22\text{-}B5}/Poxn^{70}$). n = 3–16. Error bars, interquartile range.

(legend continued on next page)

different between control and *Poxn* mutant flies (Figure 2A). In addition, most tested bitter compounds elicited similar degrees of food intake suppression in both *Poxn* mutants and control flies (Figure 2B), consistent with the idea that pharyngeal taste can be sufficient to mediate food intake suppression. We note that the inhibitory effects of bitter compounds on discrete parameters of food intake (i.e., meal size and meal frequency) were more variable between control and *Poxn* flies (Figures 2C–2F). For example, meal sizes for sucrose alone and for the sucrose/theophylline mixture were significantly larger in *Poxn* mutants than in control flies (Figure 2C), whereas meal frequencies for sucrose mixtures with coumarin, caffeine, and theophylline were significantly lower in *Poxn* mutants than in control flies (Figure 2E). Thus, overall food consumption appears to be normal in *Poxn* mutants, in which taste input is derived solely from the pharynx; however, discrete parameters of food intake may be influenced by other factors that are lacking or altered in these flies.

Pharyngeal GRNs Mediate Feeding Avoidance of Bitter Tastants

We next aimed to test the role of pharyngeal taste in feeding avoidance of bitter compounds because *Poxn* mutant flies, which have intact pharyngeal GRNs (Chen and Dahanukar, 2017; LeDue et al., 2015), appropriately rejected many tastants. We first silenced all pharyngeal GRNs in *Poxn* mutants by expressing an inwardly rectifying potassium channel, Kir2.1, under the control of *Ir25a-GAL4*, which labels all pharyngeal GRNs (Chen and Dahanukar, 2017). To measure food intake over 24 h in fed flies, we labeled fly food with a radioactive ^{32}P tracer (Ja et al., 2009; Deshpande et al., 2014) and quantified radiolabeled food consumption. We tested behavioral responses to two bitter compounds, namely denatonium and lobeline, which evoked comparable levels of feeding avoidance in both control and *Poxn* mutant flies (Figure 1C). In control flies, sucrose/bitter mixtures containing denatonium or lobeline almost completely abolished food intake in comparison with sucrose alone (Figure 3A). We found that *Poxn* mutants in which all pharyngeal GRNs were silenced (*Poxn; Ir25a-silenced*) consumed more sucrose over the same time frame. Notably, they also consumed larger amounts of the sucrose/bitter mixtures, a phenotype consistent with that of bitter-insensitive flies. Nonetheless, intake of sucrose/bitter mixtures in *Ir25a-silenced Poxn* flies was less than that observed for sucrose alone (Figure 3A), suggesting a possible involvement of post-ingestive mechanisms that operate over the 24-h time frame of this consumption assay. Therefore, we compared bitter feeding avoidance of *Ir25a-silenced Poxn* and control flies in short-term (2-h) binary choice assays. We found that avoidance of both bitter tastants was significantly reduced in *Ir25a-silenced Poxn* flies compared to some transgenic controls, barring two exceptions in which denatonium avoidance was not significantly different between *Ir25a-silenced* and *Ir25a-GAL4* control flies (Kruskal-Wallis, uncorrected Dunn's test, p = 0. 0892) and lobeline avoidance was not significantly different between *Ir25a-silenced* and *UAS-Kir2.1* control flies (Kruskal-Wallis, uncorrected Dunn's test, p = 0. 0853) (Figure 3B). However, the preference indices of *Ir25a-silenced Poxn* flies were not significantly different from zero (Wilcoxon signed rank test, p = 0.5542 for denatonium and p = 0.5186 for lobeline). In fact, behavioral responses of *Ir25a-silenced Poxn* flies in tests with sucrose alone were no different from those in tests with sucrose/bitter mixtures, consistent with a complete loss of feeding preference for higher concentration of sugars and avoidance of sugar/bitter mixtures in these assays.

Given that *Gr66a* is broadly expressed in external bitter GRNs and is required for responses to many bitter tastants (Wang et al., 2004; Thorne et al., 2004), we next asked whether pharyngeal *Gr66a* neurons are necessary for feeding avoidance of denatonium and lobeline. We also investigated *Gr93d* neurons, which partially overlap with the *Gr66a* neurons (Chen and Dahanukar, 2017). We expressed Kir2.1 to genetically silence either or both *Gr66a* and *Gr93d* neurons in a *Poxn* mutant background and tested behavioral responses to denatonium and lobeline in food consumption and choice assays. We found that silencing pharyngeal *Gr66a* neurons but not *Gr93d* neurons significantly increased consumption of sucrose/bitter mixtures containing denatonium or lobeline compared to control flies (Figure 3C). The effect of silencing both *Gr66a* and *Gr93d* neurons was no different from silencing *Gr66a* neurons alone (Figure 3C), suggesting that *Gr93d* neurons may play little if any role in the suppression of food intake. In feeding preference assays, we found that behavioral avoidance of both denatonium and lobeline was significantly reduced in *Gr66a-silenced* flies compared to both *GAL4* and *UAS* transgenic controls (Figure 3D). Unexpectedly, we observed that *Gr93d-silenced* flies displayed enhanced feeding avoidance of denatonium compared to both transgenic controls and also enhanced feeding avoidance of lobeline compared to *UAS* control. Altogether, our results suggest that pharyngeal *Gr66a* GRNs mediate both negative preference for and intake suppression of bitter compounds.

Pharyngeal GRNs Regulate Distinct Meal Parameters to Suppress Food Intake

We next tested whether acute activation of pharyngeal GRNs only during feeding events is sufficient for the suppression of food intake. We elected to test two different *Gr66a* pharyngeal GRNs that are specifically labeled by *GAL4* drivers that are not expressed in external taste organs. These are the V5 (*Gr77a-GAL4*) and the V6 (*Gr9a-GAL4*) neurons. We also tested the L7-3 (*Gr23a-GAL4*) neuron, which is one of the pharyngeal neurons that co-expresses *Gr93d*. We modified the ARC assay to collect meals from freely feeding fed flies while acutely activating

(E) Scale depicting log[IA] values for tested bitter compounds in control (top) and *Poxn* mutant flies (bottom). Compounds are labeled as "pharynx-sensitive" or "pharynx-insensitive" based on an arbitrary cutoff at a value of –0.25 for the slopes (*m*) of trend lines derived from linear regression analyses for *Poxn* mutant data shown in (C) and (D).

(F) A plot of log[IA] derived from *Poxn* flies versus control flies. The red line indicates the trend line derived from linear regression analysis.

In all plots: CAF, caffeine; COU, coumarin; DEET, N,N-diethyl-meta-toluamide; DEN, denatonium; LOB, lobeline; PAP, papaverine; QUI, quinine; STR, strychnine; TA, tartaric acid; TPH, theophylline.

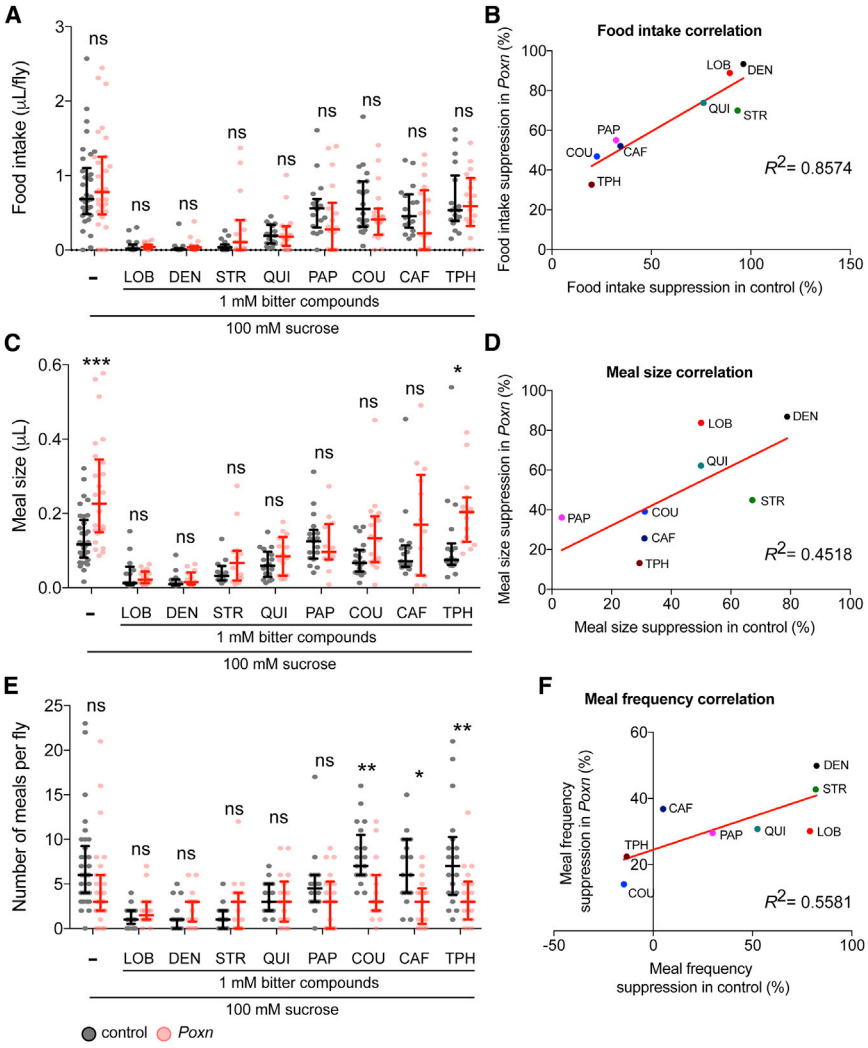

Figure 2. *Poxn* Flies Display Suppression of Food Intake by Aversive Tastants

(A, C, and E) Total food intake (A), meal size (C), and meal frequency (E) of individual flies to 100 mM sucrose alone or 100 mM sucrose with 1 mM bitter mixtures from individual flies over a 24-h period. *p < 0.05, **p < 0.01, ***p < 0.001 versus control, two-way ANOVA with post hoc Sidak's multiple comparisons test. ns, not significant.

(B, D, and F) Comparisons of food intake (B), meal size (D), and meal frequency (F) derived from *Poxn* flies versus control flies. Red lines indicate trend lines derived from linear regression analyses. Genotypes were control (w^{1118}) and *Poxn* ($Poxn^{\Delta M22\text{-}B5}/Poxn^{70}$). n = 12–34. Error bars, interquartile range.

the GRNs by expressing red-shifted channelrhodopsins (*UAS-CsChrimson*) (Klapoetke et al., 2014) under the control of the three *GAL4* drivers. Importantly, the optogenetic activation of the GRNs was tied to consumption events, as the onset of the light stimulus was triggered by automated detection of ingestion (Figures 4A and 4D). We offered these transgenic flies 100 mM sucrose and measured meal size and the average time to the next meal with or without light stimulation (Figures 4A and 4D). Interestingly, activation of *Gr9a* GRNs significantly decreased meal size compared to that in counterparts who were feeding without light stimulation (Figure 4B). However, *Gr9a* GRN activation had no effect on the time to the next meal (Figure 4C). By contrast, activation of either *Gr23a* or *Gr77a* GRNs delayed the initiation of the subsequent meal without changing meal size (Figures 4B and 4C). *UAS-CsChrimson* transgenic control flies showed no difference, both in meal size and average time to the next meal, upon light stimulation (Figures 4B and 4C). Thus, activation of a single pharyngeal *Gr66a* GRN is sufficient to suppress meal size. Moreover, our findings suggest that distinct classes of putative bitter-sensing pharyngeal GRNs may suppress overall food intake by regulating different aspects of microfeeding behaviors.

Functional Redundancies in Pharyngeal GRNs for Sensing Aversive Tastants

Thus far, our results showed that feeding avoidance of sucrose/bitter mixtures is not completely lost in *Gr66a-silenced Poxn* flies (Figure 3D) because silencing *Gr66a* neurons did not completely restore preference indexes to positive values typically observed for 5 mM sucrose alone. These data raise the possibility that other classes of pharyngeal GRNs are involved. To identify such classes of pharyngeal GRNs, we tested the roles of different subsets of pharyngeal GRNs labeled by 8 different *chemosensory receptor-GAL4* drivers (Chen and Dahanukar, 2017). We systematically tested each of these *Gr/Ir-silenced Poxn* flies in feeding preference assays by using a mixture of 2 mM sucrose and 1 mM denatonium against 2 mM sucrose alone (Figure S1A). We found that silencing of any one type of pharyngeal GRN did not cause a significant reduction in feeding avoidance of sucrose mixed with denatonium (Figure S1A). Similar results were obtained when testing the effect of silencing these different pharyngeal GRNs in feeding choice assays using a mixture of 2 mM sucrose and 10% tartaric acid (Figure S1B) or 500 mM NaCl (Figure S1C) against 2 mM sucrose alone.

Aversive Tastants Inhibit Pharyngeal *Gr43a* but Not *Ir60b* GRNs

We hypothesized that inhibition of appetitive *Gr43a* pharyngeal GRNs by aversive tastants might contribute to feeding avoidance. Recordings from external taste bristles have demonstrated that various aversive tastants can inhibit sugar-evoked responses in external sugar-sensing GRNs (French et al., 2015; Jeong et al., 2013; Charlu et al., 2013). To directly examine whether aversive compounds can inhibit sugar-induced activity

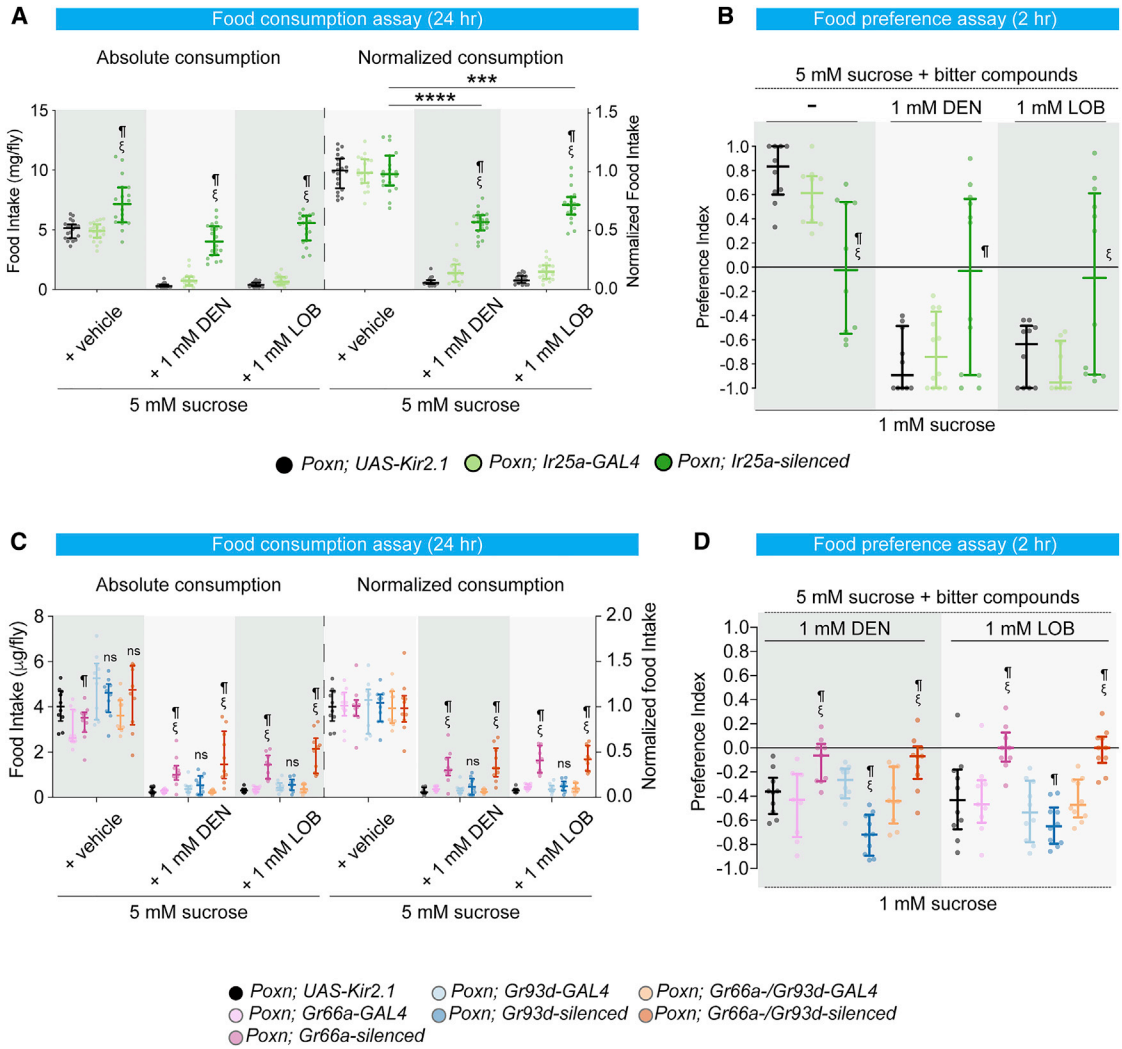

Figure 3. Pharyngeal GRNs Are Required for Intake Suppression and Feeding Avoidance of Bitter Compounds

(A and C) Food intake measurement for 5 mM sucrose alone or mixed with 1 mM bitter compounds over a 24-h period. The absolute food intake shown on the left was normalized to vehicle control as normalized food intake shown on the right. n = 10–20. Error bars, interquartile range. All genetic manipulations with *Ir25a-GAL4* (A) and *Gr66a-GAL4*, *Gr93d-GAL4* (C) were performed in a *Poxn* mutant background ($Poxn^{\Delta M22\text{-}B5}/Poxn^{70}$). ¶ and ξ indicate a statistically significant difference from the *UAS* and *GAL4* controls, respectively, by two-way ANOVA followed by Tukey's multiple comparison test. ***$p < 0.001$, ****$p < 0.0001$ versus vehicle, one-way ANOVA with post hoc Tukey's multiple comparisons test in *Poxn, Ir25a-silenced* flies.

(B and D) Feeding preference for 5 mM sucrose mixed with 1 mM denatonium or lobeline against 1 mM sucrose is shown on a scale of −1 to +1. n = 9–12. Error bars, interquartile range. All genetic manipulations with *Ir25a-GAL4* (B) and *Gr66a-GAL4*, *Gr93d-GAL4* (D) were performed in a *Poxn* mutant background ($Poxn^{\Delta M22\text{-}B5}/Poxn^{70}$). ¶ and ξ indicate a statistically significant difference from the *UAS* and *GAL4* controls, respectively, by one-way ANOVA followed by uncorrected Fisher's least significant difference (LSD) test or Kruskal-Wallis test followed by uncorrected Dunn's test. A one sample t test or Wilcoxon signed-rank test was used to test whether the median values for each genotype were different from zero.

See also Figure S1.

in pharyngeal *Gr43a* GRNs, we expressed the calcium indicator, GCaMP6s, in *Gr43a* GRNs and measured fluorescence changes in labeled neurons in the labral sense organ (LSO) after tastant application in an *ex vivo* pharyngeal imaging preparation (Joseph et al., 2017) (Figures 5A and S2).

Consistent with our earlier report (LeDue et al., 2015), pharyngeal *Gr43a* GRNs showed robust activation in response to 1 M sucrose (Figure 5A). Notably, the response was nearly abolished when any one of the three aversive tastants were included in the stimulus solution. Denatonium (Figures 5B and 5E), tartaric acid (Figures 5C and 5F), and salt (Figures 5D and 5G) were each tested at two different concentrations, both of which caused strong inhibition. Analysis of calcium activity over time revealed dose-dependent differences in the strength of inhibition. For example, although 100 mM denatonium eliminated activation by 1 M sucrose, the addition of a lower concentration of denatonium (10 mM) still allowed for weak calcium activity (ΔF/F 31% ± 9%, SEM, n = 11; p = 0.0104, Mann-Whitney test versus water,

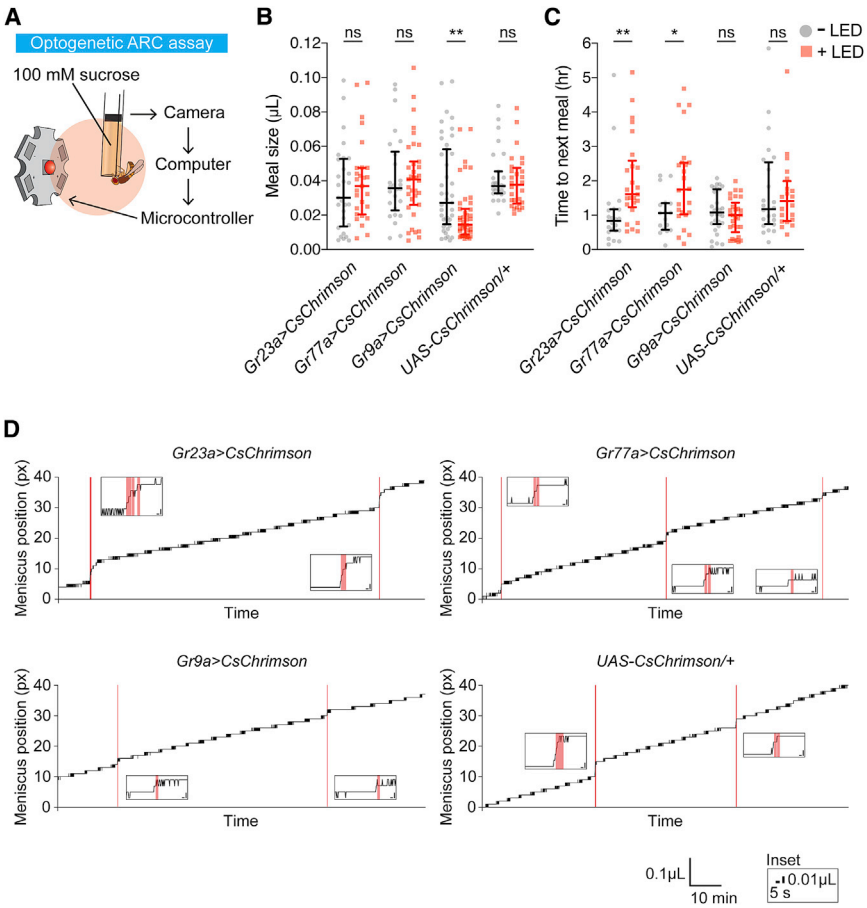

Figure 4. Pharyngeal Bitter GRNs Control Different Parameters of Micro-feeding Behaviors to Suppress Food Intake

(A) Schematic diagram of optogenetic ARC showing the setup for closed-looped optical activation of pharyngeal GRNs. Food intake of individual flies is tracked by the computer in real time. When the meniscus of the liquid food drops over a predetermined threshold, a microcontroller turns on the 625 nm light-emitting diode (LED) for 5 s.

(B–D) *UAS-CsChrimson* was expressed in single pharyngeal GRNs labeled by *Gr23a-GAL4*, *Gr77a-GAL4*, and *Gr9a-GAL4* in a wild-type background.

(B and C) Meal sizes (B) and intermeal intervals (C) were analyzed. The –LED and +LED groups of the same genotype were compared using two-way ANOVA followed by post hoc Sidak's multiple comparisons test. ns, not significant. n = 17–43. *p < 0.05, **p < 0.01.

(D) Sample traces of meniscus level tracked over time. A step-like jump in the vertical position of the meniscus represents a feeding event. The red lines indicate the activation of 625 nm LED triggered by food consumption.

n = 11–19). We note that all aversive tastants caused a sustained depression of GCaMP6 signal below the pre-stimulus baseline of fluorescent activity, possibly due to the continuous contact with the tastant, once delivered by our perfusion method. The dynamics of depression appeared to be concentration-dependent, with faster depression occurring at higher concentrations of aversive tastants (Figures 5B–5G).

To investigate whether bitter tastants can inhibit other sugar-sensing pharyngeal GRNs, we imaged stimulus-evoked calcium activity in pharyngeal *Ir60b* GRNs, which respond to sugars and act to limit consumption (Joseph et al., 2017). We used a stronger transgenic driver, *Ir94f-GAL4*, to label the pharyngeal *Ir60b* GRNs in LSO and found that application of 100 mM sucrose elicited a significant elevation in GCaMP6 fluorescence compared to water (Figures 5H and S3), consistent with the previous results (Joseph et al., 2017). Notably, inclusion of 10 mM denatonium did not affect the response to sucrose. However, we observed a significant change in calcium activity with 10 mM denatonium alone, suggesting that *Ir60b* GRNs are activated by bitter tastants in addition to sweet tastants. Although the role of *Ir60b* GRNs in feeding response to aversive tastants alone has not been evaluated, the imaging results are consistent with the negative behavioral role of *Ir60b* GRNs in limiting food consumption. We also noticed some differences in the temporal dynamics of *Gr43a* and *Ir60b* GRN responses; those in the latter were delayed and remained sustained for longer periods of time compared to *Gr43a* GRNs (Figures 5I and S3), in agreement with previous findings (Joseph et al., 2017; LeDue et al., 2015). Overall, our results demonstrate that various categories of aversive tastants can inhibit the activity of pharyngeal *Gr43a* but not *Ir60b* GRNs. In addition, pharyngeal *Ir60b* GRNs sense tastants of at least two different categories.

Distinct Combinations of Pharyngeal GRNs Mediate Feeding Avoidance of Different Tastants

We next considered that the inhibition of pharyngeal *Gr43a* GRN activity (Figure 5) may contribute to behavioral outcomes in binary choice assays and potentially eclipse the roles of other classes of GRNs in feeding avoidance of aversive tastants. We hypothesized that by simultaneously silencing *Gr66a* neurons, which could be activated by bitter compounds, and *Gr43a* neurons, which are subject to bitter-compound-mediated inhibition, we could completely abolish aversion to bitter tastants. Thus, we systematically tested double-silenced flies in which selected neuronal types were silenced in combination with all pharyngeal sweet GRNs labeled by *Gr64e-GAL4*, which is expressed in *Gr43a* GRNs. Indeed, we found that silencing both *Gr64e* and *Gr66a* GRNs abolished avoidance of denatonium (PI was not significantly different from zero, Wilcoxon signed rank test, p = 0.1774), suggesting that flies lose the ability to sense denatonium when both *Gr64e*- and *Gr66a*-dependent mechanisms are ablated. Similar effects were not observed with any other *Gr64e/GrX or IrX* doubled-silenced flies, except for *Ir76b-silenced* flies in which all *Gr64e* GRNs as well as 13

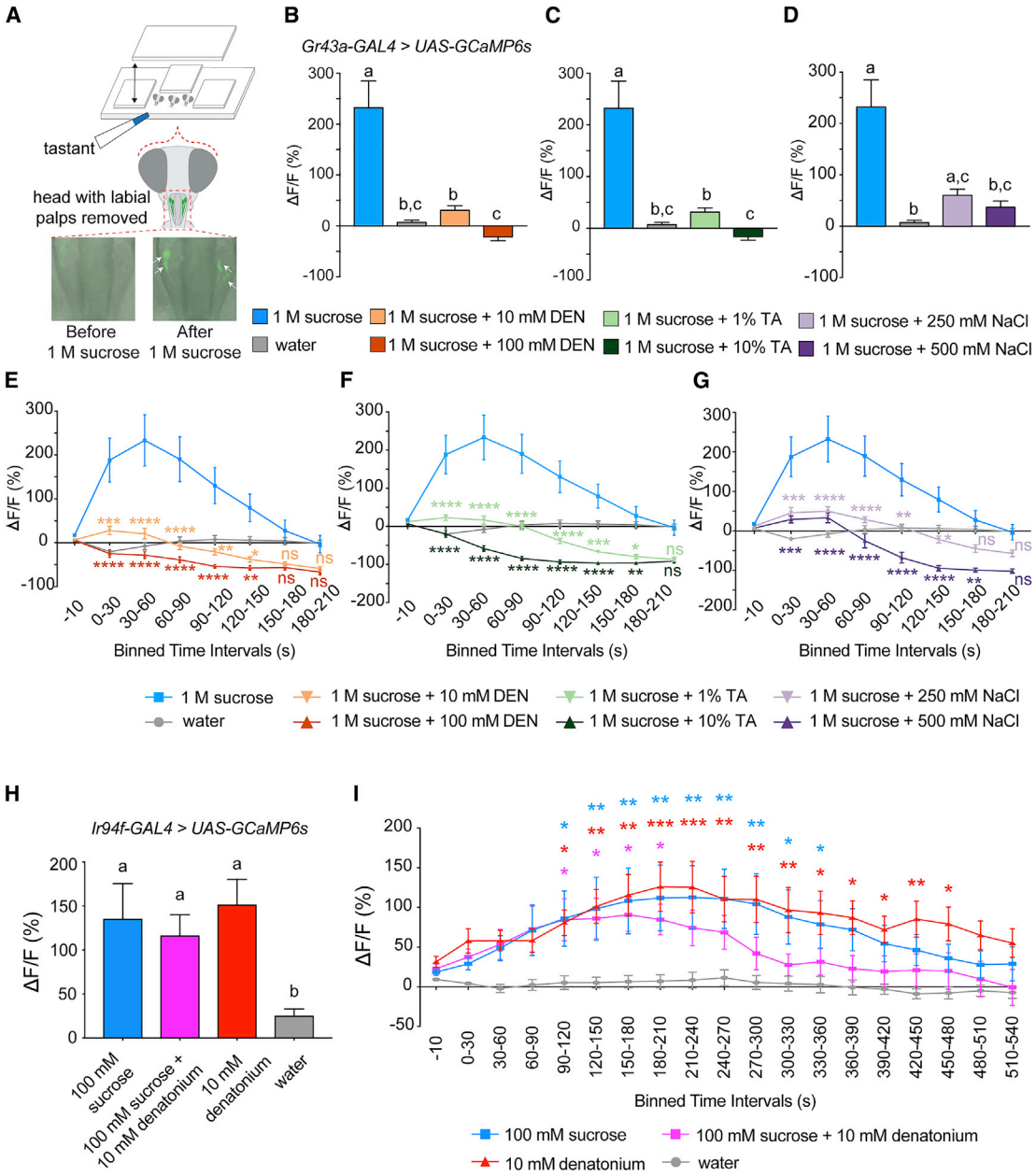

Figure 5. Calcium Imaging Shows That Aversive Tastants Inhibit the Activity of Pharyngeal *Gr43a* GRNs

(A) Schematic diagram of the *ex vivo* pharyngeal calcium imaging setup (top). Flies expressing GCaMP6s calcium indicator in pharyngeal *Gr43a* GRNs were imaged by confocal microscopy. Representative fluorescence images of pharyngeal *Gr43a* GRNs in the LSO before and after 1 M sucrose stimulus (bottom). Arrows indicate the cell bodies of the pharyngeal *Gr43a* GRNs.

(B–D) Peak changes of GCaMP6s fluorescence in pharyngeal *Gr43a* GRNs to 1 M sucrose alone or mixed with 10 mM or 100 mM denatonium (B), 1% or 10% tartaric acid (C), or 250 mM or 500 mM NaCl (D). Different letters indicate significantly different groups by Kruskal-Wallis test followed by Dunn's multiple comparison test. n = 11–28. Error bars, SEM.

(E–G) Time course of change in fluorescence (ΔF/F) for samples stimulated with mixtures of sucrose and denatonium (E), tartaric acid (F), or salt (G). ΔF/F values are binned into 30-s intervals after application of stimulus. Asterisks indicate significant difference from 1 M sucrose by two-way ANOVA followed by Tukey post hoc test. *$p < 0.05$, **$p < 0.01$, ***$p < 0.001$, ****$p < 0.0001$.

(H) Peak changes of GCaMP6s fluorescence in pharyngeal *Ir60b* GRNs labeled by *Ir94f-GAL4* to 100 mM sucrose alone, mixture of 100 mM sucrose with 10 mM denatonium, or 10 mM denatonium alone. Different letters indicate significantly different groups by Kruskal-Wallis test followed by Dunn's multiple comparison test. n = 8–10. Error bars, SEM.

(I) Time course of change in fluorescence (ΔF/F) for samples that received indicated stimuli. ΔF/F values are binned into 30-s intervals after application of stimulus. Asterisks indicate significant difference from water alone by two-way ANOVA followed by Tukey post hoc test. *$p < 0.05$, **$p < 0.01$, ***$p < 0.001$.

See also Figures S2 and S3.

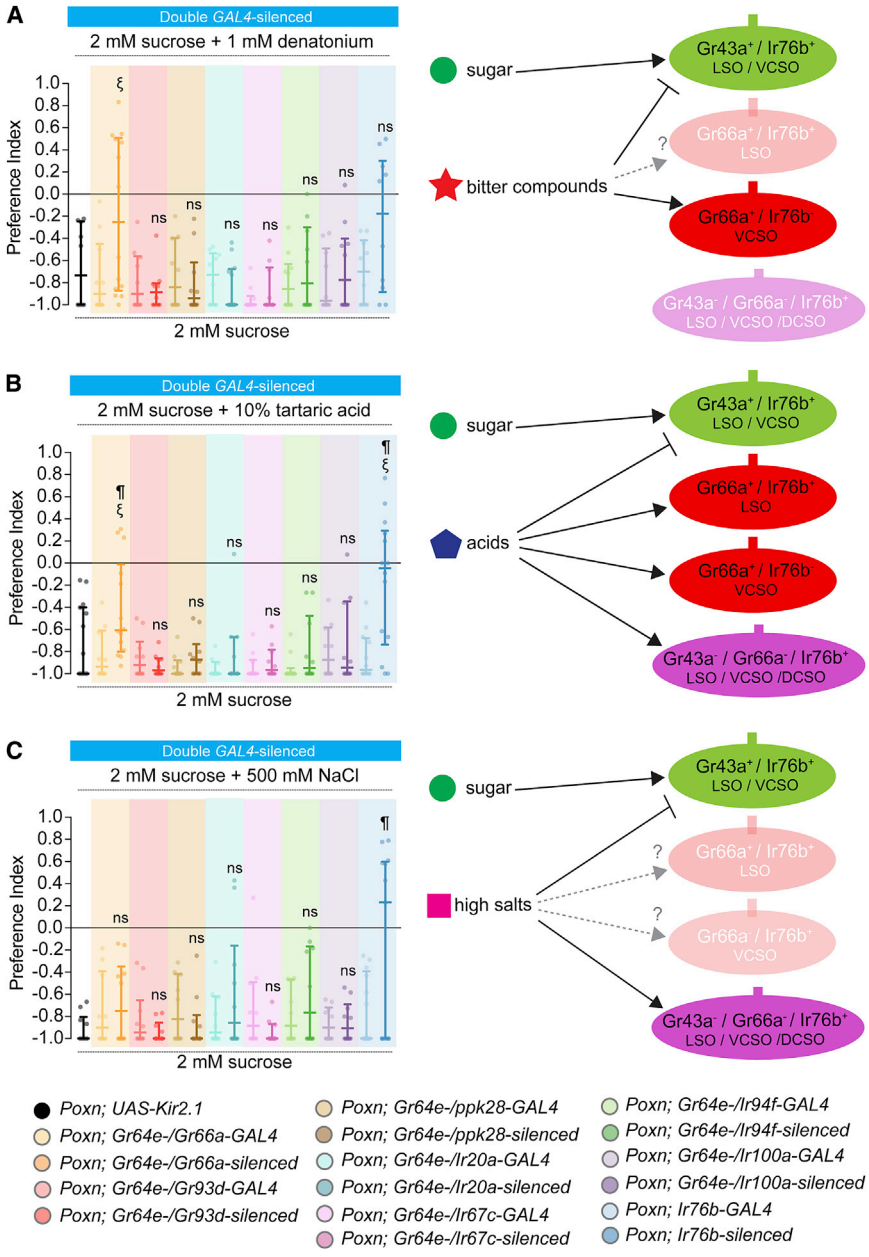

Figure 6. Distinct Combinations of Pharyngeal GRNs Are Required for Feeding Avoidance of Different Aversive Tastants

(A–C) Mean preference index values of *Poxn* (*Poxn*$^{\Delta M22\text{-}B5}$/*Poxn*^{70}) mutants carrying indicated transgenes obtained from binary choice experiments with 2 mM sucrose mixed with 1 mM denatonium (A), 10% tartaric acid (B), or 500 mM NaCl (C) tested against 2 mM sucrose alone. *UAS-Kir2.1* and *Gr/Ir-GAL4* transgenes were tested independently as indicated or together (*Gr/Ir-silenced*). The schematics on the right depict how bitter compounds, tartaric acid, and high salts are each detected by multiple classes of pharyngeal GRNs. The oval shapes depict different classes of pharyngeal GRNs, defined by the chemosensory receptor expression from our previous study (Chen and Dahanukar, 2017). LSO, labral sense organ; VCSO, ventral cibarial sense organ; DCSO, dorsal cibarial sense organ. n = 10–15. Error bars, interquartile range. ¶ and ξ indicate a statistically significant difference from the *UAS* and *GAL4* controls, respectively, by one-way ANOVA followed by uncorrected Fisher's LSD test or Kruskal-Wallis test followed by uncorrected Dunn's test. The one-sample t test or Wilcoxon signed-rank test was used for testing whether the median values for each genotype were different from zero.

additional pharyngeal GRNs were functionally abolished (Wilcoxon signed rank test, p = 0.2656) (Figure 6A).

Next, we aimed to identify the classes of pharyngeal GRNs involved in mediating tartaric acid avoidance. As expected from the results of calcium imaging, when both *Gr64e* and *Gr66a* GRNs were silenced, we observed a significant reduction in feeding avoidance of 10% tartaric acid (Figure 6B). In this instance, *Gr64e-/Gr66a-silenced Poxn* flies retain some ability to avoid tartaric acid (PI was significantly different from zero, Wilcoxon signed rank test, p = 0.0085), invoking a role for at least one additional class of *Ir76b* GRNs because silencing all *Ir76b* pharyngeal GRNs abolished tartaric acid avoidance (PI was not significantly different from zero, Wilcoxon signed rank test, p = 0.3696).

Finally, we performed similar analyses to identify pharyngeal GRNs that underlie feeding avoidance of 500 mM salt (Figure 1B). Surprisingly, none of the tested combinations of *Gr64e* sweet GRNs and other subsets of GRNs were sufficient to eliminate avoidance of high salt (Figure 6C). Salt avoidance was abolished only when all *Ir76b* pharyngeal GRNs were silenced, signaling broader functional redundancies for high salt avoidance. Together, our results suggest that multiple classes of taste neurons are involved in driving behavioral responses to aversive tastants. Moreover, different categories of aversive tastants may be sensed by overlapping but distinct groups of GRNs. Overall, our results imply a greater degree of functional overlap in these pharyngeal neurons than previously appreciated.

Tracing Second-Order Pharyngeal Taste Circuits Reveals Two Main Taste Centers in the Brain Connecting with Pharyngeal GRNs

To understand how pharyngeal taste information is represented at the second relay, we used the newly developed circuit tracing technique trans-Tango (Talay et al., 2017) in combination with the molecular toolkit for labeling subsets of pharyngeal GRNs in *Poxn* mutant flies. By recombining trans-Tango cassettes with the *Poxn*^{70} mutant allele, we were able to specifically trace pharyngeal second-order neurons. We first performed

experiments to trace circuits of pharyngeal *Gr32a* bitter GRNs. Notably, the number of *Gr32a* second-order neurons labeled in the brain of a *Poxn* mutant (~20–30) was greatly reduced compared to that in a wild-type brain (> 100) (Figures 7A and 7Ai), presenting a numerically tractable model for characterizing the anatomy of taste circuits. We noticed that neurons lying above the antennal lobes were not labeled in the *Poxn* flies and, thus, are likely to be specifically connected with external *Gr32a* GRNs. In addition, second-order neurons connected to pharyngeal *Gr32a* GRNs, or subsets thereof, (Figures 7Aii and 7Aiii) showed projections to two main brain regions, namely, pars intercerebralis and lateral protocerebrum. Labeling of second-order neuronal circuits for all possible pharyngeal GRNs showed that most, if not all, projected to these two brain regions (Figures 7A–7C), implicating them as potential relay centers for pharyngeal taste inputs.

Some of the *GAL4* lines (*Gr9a-*, *Gr23a-*, *Ir67c-*, and *Ir94f-GAL4*) used for trans-Tango tracing exclusively labeled single identified pharyngeal neurons (Chen and Dahanukar, 2017), offering the opportunity to examine the number of second-order taste neurons connected to a single pair of pharyngeal GRNs. We found that each of these neurons connected with multiple second-order neurons (at least 10) and labeled projections in the pars intercerebralis and lateral protocerebrum (Figures 7Aiii, 7C, 7Ciii, and 7Civ), suggesting that even a specific gustatory input may be broadly conveyed across a few distinct brain regions. Together, our results lay the foundation for further system-wide functional analyses of pharyngeal second-order neurons.

DISCUSSION

Flies have multiple taste organs in the body, present externally and internally. Taste neurons present in organs that line the pharynx have been thought to act as gatekeepers for monitoring food palatability, but they have been less studied in comparison with their external counterparts. Here, we assess the role of pharyngeal taste in driving food preference and consumption using *Poxn* mutants, which possess only a "minimal" pharyngeal taste system. We find that *Poxn* flies show behavioral sensitivity to a diverse panel of aversive compounds, including high concentrations of salt, tartaric acid, and several bitter compounds, in a manner that is similar to control flies. Notably, the intensity of feeding aversion evoked by a given bitter tastant is strongly correlated between *Poxn* and control flies, implicating pharyngeal taste as sufficient for determining feeding avoidance. We probe the contributions of pharyngeal GRN classes in feeding aversion to various tastants by using genetic dissection studies and find that avoidance of most is achieved by multiple classes of pharyngeal GRNs, including bitter, sweet, and one or more additional classes. Importantly, feeding avoidance of bitter compounds, tartaric acid, and high salts depends on different but overlapping pharyngeal GRN classes, providing a potential mechanism for pharyngeal taste to distinguish different categories of aversive compounds based on combinations of pharyngeal GRNs that are involved. We note that pharyngeal GRNs are genetically silenced throughout development, and therefore, the possibility of potential developmental defects contributing to phenotypic outcomes cannot be ruled out.

Despite extensive, systematic characterization of external taste neuronal responses to large panels of bitter compounds (Ling et al., 2014; Weiss et al., 2011), some questions remain about how these taste inputs are translated to behavior. In particular, why do some robust or broad activators of bitter taste neurons (e.g., caffeine) evoke weaker degrees of aversion in feeding assays compared to other compounds? Our results, which show that pharyngeal input plays an important role in driving avoidance of aversive tastants, offer one explanation for this conundrum. Although we found differences in the "bitterness" rank order of compounds in binary choice and consumption assays, internal taste input was sufficient for assigning bitterness values and suppressing food intake in patterns that closely resemble those observed in control flies. Features that determine aversion intensity of bitter compounds are not well understood, but a prevailing view is that bitter chemicals signal toxicity. Such a model would predict that compounds that are more toxic would be perceived as more bitter and, consequently, avoided to a greater extent. It would be interesting to investigate any potential relationship between pharyngeal sensitivity and toxicity of various bitter compounds.

Our data also suggest that external and internal taste inputs are not functionally redundant. First, even for pharynx-sensitive compounds (e.g., quinine, papaverine, and coumarin), *Poxn* mutants show reduced avoidance at higher concentrations, suggesting that information from both external and internal neurons converges to control overall feeding avoidance. Second, the contribution of external GRNs is more prominent for pharynx-insensitive compounds (e.g., caffeine, theophylline, DEET, and strychnine), suggesting a functional division of bitter taste in organs located in different parts of the body. Whether this is due to differences in activation of bitter GRNs or inhibition of sweet GRNs or both would be interesting to determine in future studies. Last, meal size and meal frequency do not correlate well between *Poxn* mutants and control flies, suggesting that these parameters may be influenced by other factors that are altered or lacking in *Poxn* mutants. We also note that some chemosensory receptors are expressed in enteroendocrine cells (Park and Kwon, 2011), and this could also contribute to feeding aversion in long-term (24-h) assays by unidentified post-ingestive mechanisms.

Previous studies have demonstrated dual mechanisms for cellular detection of aversive compounds—activation of bitter GRNs and inhibition of sweet GRNs (Jeong et al., 2013; French et al., 2015; Charlu et al., 2013). Our results posit that both of these mechanisms exist in pharyngeal GRNs as well. In contrast to a recent study of labellar salt taste, which found that high salt activates sweet neurons (*Gr64f*) (Jaeger et al., 2018), we observe that high salt can inhibit pharyngeal *Gr43a* neurons in calcium imaging experiments, suggesting an intriguing common mechanism for multiple categories of aversive compounds to inhibit neuronal activities of appetitive neurons. A previous study also showed that behavioral avoidance of bitter compounds is well correlated with the extent of sweet GRN inhibition in the labellum (Sellier et al., 2011), suggesting that sweet GRN inhibition might be a better predictor for behavioral avoidance of sugar/bitter mixtures compared to bitter GRN activation. Although we did not successfully isolate specific populations of pharyngeal neurons that mediate feeding avoidance of high salt, we provide

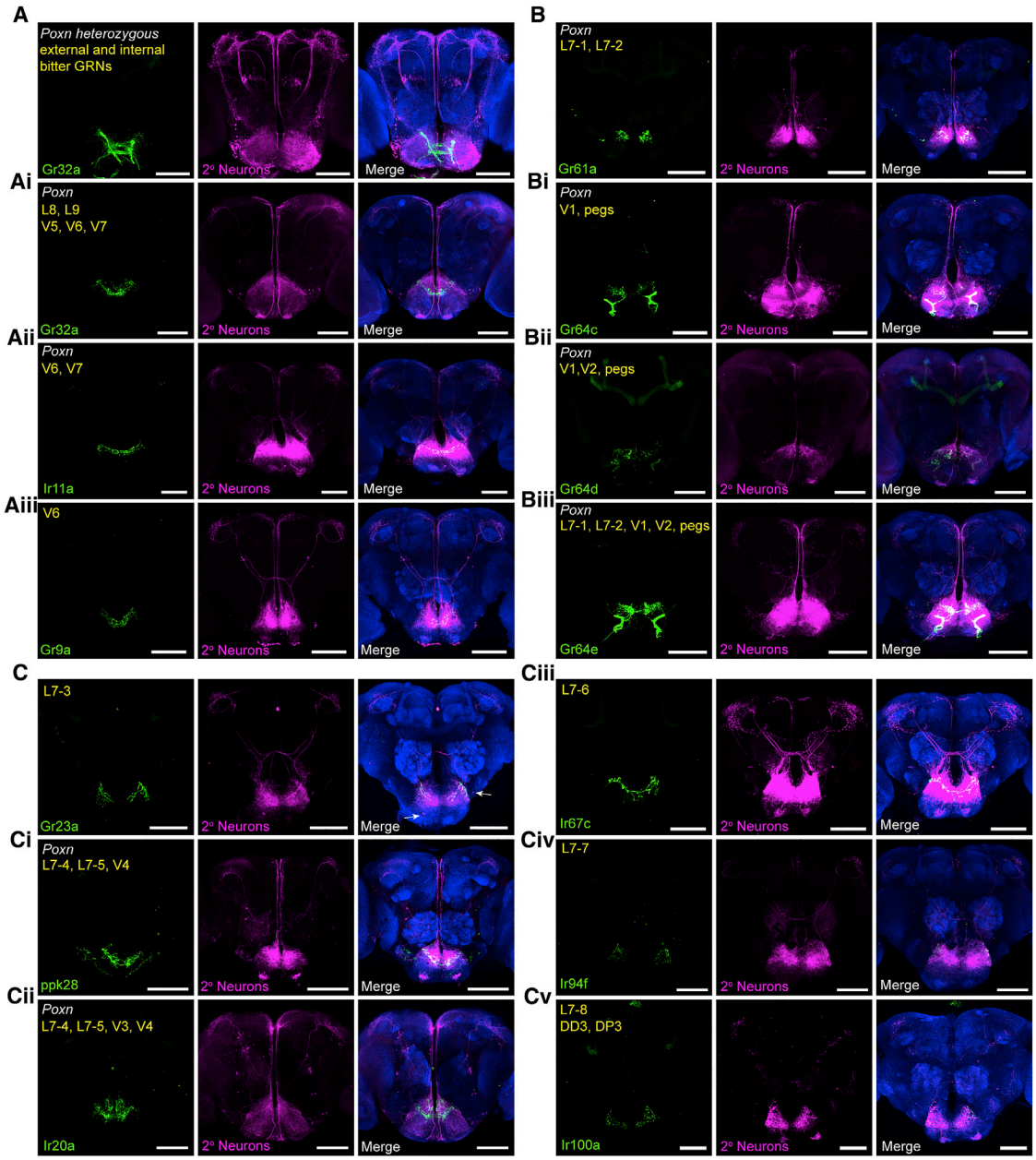

Figure 7. trans-Tango Tracing of Second-Order Pharyngeal Neurons Reveals Two Main Higher-Order Regions That Receive Taste Input

(A–D) Examples demonstrating use of trans-Tango system to map second-order taste neurons (magenta) that connect with bitter (A), sweet (B), or other classes (C and D) of pharyngeal GRNs (green). The nomenclature of pharyngeal GRNs established in our previous study was used (Chen and Dahanukar, 2017). Note the reduced number of second-order taste neurons labeled in *Poxn*/*Poxn* homozygous versus *Poxn*/+ heterozygous backgrounds (A and Ai). Unless otherwise noted as *Poxn*, staining was performed in a wild-type background for some drivers, such as *Gr9a*-, *Gr23a*-, *Ir67c*-, *Ir94f*-, and *Ir100a-GAL4*.

evidence that sweet neurons and other *Ir*-expressing neurons are both required for full feeding avoidance of high salt in our behavioral assays. Unlike those of external GRNs (Delventhal et al., 2014; Ling et al., 2014; Weiss et al., 2011; Marella et al., 2006; Shankar et al., 2016), physiological responses of pharyngeal GRNs have not been well studied, in large part due to their inaccessible location for electrophysiological analyses and the necessity of active ingestion for the purposes of calcium imaging of presynaptic terminals (Benton and Dahanukar, 2011; LeDue et al., 2015). New methods that allow for assessing the sensitivity and receptivity of pharyngeal GRNs and comparing the tastant spaces sampled by internal and external organs would be invaluable.

By focusing on the minimal pharyngeal taste system, we created a map of pharyngeal inputs and their corresponding second-order pharyngeal taste neurons by using the newly

developed circuit-tracing technique trans-Tango (Talay et al., 2017). We show that pharyngeal second-order neurons convey information to areas (pars intercerebralis and lateral protocerebrum) that also receive external taste input. Thus, pharyngeal taste circuits offer a tractable model to analyze the anatomy and function of taste circuitry and its intersections with higher-order brain functions. Notably, several neuroendocrine cells in the pars intercerebralis, including insulin-producing cells (IPCs), DH44, and SIFamidergic neurons, have been implicated in nutrient-sensing and feeding behaviors (Martelli et al., 2017; Yang et al., 2018; Dus et al., 2015; Söderberg et al., 2012; Broughton et al., 2010). The smaller numbers of pharyngeal second-order neurons uncovered in our study would facilitate future functional analyses of response properties of second-order taste neurons and their anatomical connectivity with brain neuroendocrine/nutrient-sensing cells.

Among GRNs, those residing in the pharynx are unique because a subset of them persist through metamorphosis (Gendre et al., 2004). Thus, the pharynx may represent a unique site where information about sensory experience is maintained and transferred from the larval stages to adult stage. Interestingly, taste neurons in the pharynx, but not in other taste organs, regulate oviposition preference for non-appetitive substrates (Joseph and Heberlein, 2012), indicating that flies are capable of remembering a previously encountered non-appetitive substrate to which they return to lay eggs. It would be of interest to examine trans-metamorphic taste memory in flies and pinpoint the involvement of specific pharyngeal GRNs. Future studies in this direction would yield insight into peripheral taste coding and may also lead to the discovery of novel deterrent compounds for controlling insect disease vectors and agricultural pests in a manner that abolishes the need to apply repellants or pesticides continually.

STAR★METHODS

Detailed methods are provided in the online version of this paper and include the following:

- KEY RESOURCES TABLE
- LEAD CONTACT AND MATERIALS AVAILABILITY
- EXPERIMENTAL MODEL AND SUBJECT DETAILS
  - Drosophila melanogaster
- METHOD DETAILS
  - Binary Choice Feeding Assays
  - Activity-Recording CAFE Assay (ARC)
  - Optogenetic-Activity-Recording CAFE Assay (Optogenetic-ARC)
  - Radiolabeled Food Intake Measurement
  - Calcium Imaging
  - trans-Tango
- QUANTIFICATION AND STATISTICAL ANALYSIS
- DATA AND CODE AVAILABILITY

SUPPLEMENTAL INFORMATION

Supplemental Information can be found online at https://doi.org/10.1016/j.celrep.2019.09.036.

ACKNOWLEDGMENTS

We thank Keith R. Murphy, who developed the Optogenetic ARC assay and provided technical assistance for the optogenetic ARC experiments prior to publication of the protocol, and Barbara Jablonska for technical help. Stocks were also obtained from the Bloomington *Drosophila* Stock Center (NIH P40OD018537). This work was funded by grants from the NIH (R01DC013587 to A.A.D. and R01AG045036 to W.W.J.) and funds from the UC AES Mission Funding Program. Y.-C.D.C. is a Howard Hughes Medical Institute International Student Research Fellow. S.J.P. is supported by The Celia Lipton Farris and Victor W. Farris Foundation Graduate Student Fellowship.

AUTHOR CONTRIBUTIONS

Conceptualization, Y.-C.D.C. and A.A.D.; Methodology, Y.-C.D.C., S.J.P., R.M.J., W.W.J., and A.A.D.; Investigation, Y.-C.D.C., S.J.P., and R.M.J.; Validation, Y.-C.D.C., S.J.P., and R.M.J.; Formal Analysis, Y.-C.D.C. and S.J.P.; Writing – Original Draft, Y.-C.D.C., Writing – Review & Editing, Y.-C.D.C., S.J.P., R.M.J., W.W.J., and A.A.D.; Visualization, Y.-C.D.C. and S.J.P.; Supervision, W.W.J. and A.A.D.; Funding Acquisition, W.W.J. and A.A.D.

DECLARATION OF INTERESTS

The authors declare no competing interests.

Received: August 2, 2018
Revised: August 18, 2019
Accepted: September 12, 2019
Published: October 22, 2019

REFERENCES

Awasaki, T., and Kimura, K. (1997). pox-neuro is required for development of chemosensory bristles in Drosophila. J. Neurobiol. *32*, 707–721.

Benton, R., and Dahanukar, A. (2011). Electrophysiological recording from Drosophila taste sensilla. Cold Spring Harb. Protoc. *2011*, 839–850.

Boll, W., and Noll, M. (2002). The Drosophila Pox neuro gene: control of male courtship behavior and fertility as revealed by a complete dissection of all enhancers. Development *129*, 5667–5681.

Broughton, S.J., Slack, C., Alic, N., Metaxakis, A., Bass, T.M., Driege, Y., and Partridge, L. (2010). DILP-producing median neurosecretory cells in the Drosophila brain mediate the response of lifespan to nutrition. Aging Cell *9*, 336–346.

Cameron, P., Hiroi, M., Ngai, J., and Scott, K. (2010). The molecular basis for water taste in Drosophila. Nature *465*, 91–95.

Charlu, S., Wisotsky, Z., Medina, A., and Dahanukar, A. (2013). Acid sensing by sweet and bitter taste neurons in Drosophila melanogaster. Nat. Commun. *4*, 2042.

Chen, Y.D., and Dahanukar, A. (2017). Molecular and Cellular Organization of Taste Neurons in Adult Drosophila Pharynx. Cell Rep. *21*, 2978–2991.

Chen, Y.D., Park, S.J., Ja, W.W., and Dahanukar, A. (2018). Using *Pox-Neuro* (*Poxn*) Mutants in *Drosophila* Gustation Research: A Double-Edged Sword. Front. Cell. Neurosci. *12*, 382.

Delventhal, R., Kiely, A., and Carlson, J.R. (2014). Electrophysiological recording from Drosophila labellar taste sensilla. J. Vis. Exp., e51355.

Deshpande, S.A., Carvalho, G.B., Amador, A., Phillips, A.M., Hoxha, S., Lizotte, K.J., and Ja, W.W. (2014). Quantifying Drosophila food intake: comparative analysis of current methodology. Nat. Methods *11*, 535–540.

Dus, M., Lai, J.S., Gunapala, K.M., Min, S., Tayler, T.D., Hergarden, A.C., Geraud, E., Joseph, C.M., and Suh, G.S. (2015). Nutrient Sensor in the Brain Directs the Action of the Brain-Gut Axis in Drosophila. Neuron *87*, 139–151.

Freeman, E.G., and Dahanukar, A. (2015). Molecular neurobiology of Drosophila taste. Curr. Opin. Neurobiol. *34*, 140–148.

French, A.S., Sellier, M.J., Ali Agha, M., Guigue, A., Chabaud, M.A., Reeb, P.D., Mitra, A., Grau, Y., Soustelle, L., and Marion-Poll, F. (2015). Dual mechanism for bitter avoidance in Drosophila. J. Neurosci. *35*, 3990–4004.

Gendre, N., Lüer, K., Friche, S., Grillenzoni, N., Ramaekers, A., Technau, G.M., and Stocker, R.F. (2004). Integration of complex larval chemosensory organs into the adult nervous system of Drosophila. Development *131*, 83–92.

Ja, W.W., Carvalho, G.B., Zid, B.M., Mak, E.M., Brummel, T., and Benzer, S. (2009). Water- and nutrient-dependent effects of dietary restriction on Drosophila lifespan. Proc. Natl. Acad. Sci. USA *106*, 18633–18637.

Jaeger, A.H., Stanley, M., Weiss, Z.F., Musso, P.Y., Chan, R.C., Zhang, H., Feldman-Kiss, D., and Gordon, M.D. (2018). A complex peripheral code for salt taste in *Drosophila*. eLife *7*, e37167.

Jeong, Y.T., Shim, J., Oh, S.R., Yoon, H.I., Kim, C.H., Moon, S.J., and Montell, C. (2013). An odorant-binding protein required for suppression of sweet taste by bitter chemicals. Neuron *79*, 725–737.

Joseph, R.M., and Carlson, J.R. (2015). Drosophila Chemoreceptors: A Molecular Interface Between the Chemical World and the Brain. Trends Genet. *31*, 683–695.

Joseph, R.M., and Heberlein, U. (2012). Tissue-specific activation of a single gustatory receptor produces opposing behavioral responses in Drosophila. Genetics *192*, 521–532.

Joseph, R.M., Sun, J.S., Tam, E., and Carlson, J.R. (2017). A receptor and neuron that activate a circuit limiting sucrose consumption. eLife *6*, e24992.

Kang, K., Pulver, S.R., Panzano, V.C., Chang, E.C., Griffith, L.C., Theobald, D.L., and Garrity, P.A. (2010). Analysis of Drosophila TRPA1 reveals an ancient origin for human chemical nociception. Nature *464*, 597–600.

Klapoetke, N.C., Murata, Y., Kim, S.S., Pulver, S.R., Birdsey-Benson, A., Cho, Y.K., Morimoto, T.K., Chuong, A.S., Carpenter, E.J., Tian, Z., et al. (2014). Independent optical excitation of distinct neural populations. Nat. Methods *11*, 338–346.

Koh, T.W., He, Z., Gorur-Shandilya, S., Menuz, K., Larter, N.K., Stewart, S., and Carlson, J.R. (2014). The Drosophila IR20a clade of ionotropic receptors are candidate taste and pheromone receptors. Neuron *83*, 850–865.

Kwon, J.Y., Dahanukar, A., Weiss, L.A., and Carlson, J.R. (2014). A map of taste neuron projections in the Drosophila CNS. J. Biosci. *39*, 565–574.

LeDue, E.E., Chen, Y.C., Jung, A.Y., Dahanukar, A., and Gordon, M.D. (2015). Pharyngeal sense organs drive robust sugar consumption in Drosophila. Nat. Commun. *6*, 6667.

Ling, F., Dahanukar, A., Weiss, L.A., Kwon, J.Y., and Carlson, J.R. (2014). The molecular and cellular basis of taste coding in the legs of Drosophila. J. Neurosci. *34*, 7148–7164.

Marella, S., Fischler, W., Kong, P., Asgarian, S., Rueckert, E., and Scott, K. (2006). Imaging taste responses in the fly brain reveals a functional map of taste category and behavior. Neuron *49*, 285–295.

Martelli, C., Pech, U., Kobbenbring, S., Pauls, D., Bahl, B., Sommer, M.V., Pooryasin, A., Barth, J., Arias, C.W.P., Vassiliou, C., et al. (2017). SIFamide Translates Hunger Signals into Appetitive and Feeding Behavior in Drosophila. Cell Rep. *20*, 464–478.

Murata, S., Brockmann, A., and Tanimura, T. (2017). Pharyngeal stimulation with sugar triggers local searching behavior in *Drosophila*. J. Exp. Biol. *220*, 3231–3237.

Murphy, K.R., Park, J.H., Huber, R., and Ja, W.W. (2017). Simultaneous measurement of sleep and feeding in individual Drosophila. Nat. Protoc. *12*, 2355–2366.

Nottebohm, E., Dambly-Chaudière, C., and Ghysen, A. (1992). Connectivity of chemosensory neurons is controlled by the gene poxn in Drosophila. Nature *359*, 829–832.

Park, J.H., and Kwon, J.Y. (2011). Heterogeneous expression of Drosophila gustatory receptors in enteroendocrine cells. PLoS One *6*, e29022.

Sellier, M.J., Reeb, P., and Marion-Poll, F. (2011). Consumption of bitter alkaloids in Drosophila melanogaster in multiple-choice test conditions. Chem. Senses *36*, 323–334.

Shankar, S., Calvert, M.E., and Yew, J.Y. (2016). Measuring Physiological Responses of Drosophila Sensory Neurons to Lipid Pheromones Using Live Calcium Imaging. J. Vis. Exp., 53392.

Söderberg, J.A., Carlsson, M.A., and Nässel, D.R. (2012). Insulin-Producing Cells in the Drosophila Brain also Express Satiety-Inducing Cholecystokinin-Like Peptide, Drosulfakinin. Front. Endocrinol. (Lausanne) *3*, 109.

Soldano, A., Alpizar, Y.A., Boonen, B., Franco, L., López-Requena, A., Liu, G., Mora, N., Yaksi, E., Voets, T., Vennekens, R., et al. (2016). Gustatory-mediated avoidance of bacterial lipopolysaccharides via TRPA1 activation in Drosophila. eLife *5*, e13133.

Steck, K., Walker, S.J., Itskov, P.M., Baltazar, C., Moreira, J.M., and Ribeiro, C. (2018). Internal amino acid state modulates yeast taste neurons to support protein homeostasis in *Drosophila*. eLife *7*, e31625.

Talay, M., Richman, E.B., Snell, N.J., Hartmann, G.G., Fisher, J.D., Sorkac, A., Santoyo, J.F., Chou-Freed, C., Nair, N., Johnson, M., et al. (2017). Transsynaptic Mapping of Second-Order Taste Neurons in Flies by trans-Tango. Neuron *96*, 783–795.e4.

Thorne, N., Chromey, C., Bray, S., and Amrein, H. (2004). Taste perception and coding in Drosophila. Curr. Biol. *14*, 1065–1079.

Wang, Z., Singhvi, A., Kong, P., and Scott, K. (2004). Taste representations in the Drosophila brain. Cell *117*, 981–991.

Weiss, L.A., Dahanukar, A., Kwon, J.Y., Banerjee, D., and Carlson, J.R. (2011). The molecular and cellular basis of bitter taste in Drosophila. Neuron *69*, 258–272.

Yang, Z., Huang, R., Fu, X., Wang, G., Qi, W., Mao, D., Shi, Z., Shen, W.L., and Wang, L. (2018). A post-ingestive amino acid sensor promotes food consumption in Drosophila. Cell Res. *28*, 1013–1025.

Zhang, Y.V., Ni, J., and Montell, C. (2013). The molecular basis for attractive salt-taste coding in Drosophila. Science *340*, 1334–1338.

STAR★METHODS

KEY RESOURCES TABLE

REAGENT or RESOURCE	SOURCE	IDENTIFIER
Antibodies		
Chicken anti-GFP	Abcam	Cat#ab13970; RRID: AB_300798
Rabbit anti-DsRed	Clontech	Cat#632496; RRID: AB_10013483
Mouse anti-nc82	Developmental Studies Hybridoma Bank	RRID: AB_2314866
Goat anti-Chicken IgY (H+L) Secondary Antibody, Alexa Fluor 488	Invitrogen	Cat#A11039; RRID: AB_2534096
Goat anti-Rabbit IgG (H+L) Highly Cross-Adsorbed Secondary Antibody, Alexa Fluor 568	Invitrogen	Cat#A11036; RRID: AB_10563566
Goat anti-Mouse IgG (H+L) Highly Cross-Adsorbed Secondary Antibody, Alexa Fluor 647	Invitrogen	Cat#A21236; RRID: AB_2535805
Goat serum	Sigma	Cat#G9023
Chemicals, Peptides, and Recombinant Proteins		
Sucrose	Sigma	Cat#S7903
Denatonium benzoate	Sigma	Cat#D5765
Lobeline hydrochloride	Sigma	Cat#141879
Coumarin	Sigma	Cat#4261
Quinine hydrochloride dihydrate	Sigma	Cat#22630
Papaverine hydrochloride	Sigma	Cat#P3510
Caffeine	Sigma	Cat#C8960
Theophylline	Sigma	Cat#T1633
DEET	Sigma	Cat#36542
Strychnine hydrochloride	Sigma	Cat#S8753
L-tartaric acid	Sigma	Cat#251380
Sodium chloride	Macron Chemical	Cat#7581-06
Indigo carmine	Sigma	Cat#I8130
Sulforhodamine B	Sigma	Cat#230162
all trans-retinal	Sigma	Cat#R2500
[α-32P]dCTP	PerkinElmer	Cat#NEG013H100UC
VECTASHIELD antifade mounting medium	Vector Laboratories	Cat#H-1000
Deposited Data		
All raw data	This study	http://dx.doi.org/10.17632/vj3nw2sx35.1
Experimental Models: Organisms/Strains		
D. melanogaster: w^{1118}	J. Carlson	NA
D. melanogaster: $Poxn^{\Delta M22\text{-}B5}$	M. Gordon	Boll and Noll, 2002
D. melanogaster: $Poxn^{70}$	M. Gordon	Awasaki and Kimura, 1997
D. melanogaster: Gr-GAL4	J. Carlson	Ling et al., 2014; Weiss et al., 2011
D. melanogaster: Gr66a-GAL4	Bloomington Drosophila Stock Center	BDSC#28801
D. melanogaster: Ir-GAL4	Bloomington Drosophila Stock Center	BDSC#60694; BDSC#41728; BDSC#60717; BDSC#41730; BDSC#60727; BDSC#41743; BDSC#41742; Koh et al., 2014
D. melanogaster: ppk28-GAL4	K. Scott	Cameron et al., 2010
D. melanogaster: UAS-CsChrimson	Bloomington Drosophila Stock Center	BDSC#55136
D. melanogaster: UAS-GCaMP6s	Bloomington Drosophila Stock Center	BDSC#42748
D. melanogaster: trans-Tango	G. Barnea	Talay et al., 2017
D. melanogaster: *$Poxn^{70}$, trans-Tango*	This study	NA

(*Continued on next page*)

Continued

REAGENT or RESOURCE	SOURCE	IDENTIFIER
Software and Algorithms		
GraphPad Prism 8	GraphPad Software	https://www.graphpad.com
Origin 8	OriginLab	https://www.originlab.com
Fiji	ImageJ	https://fiji.sc
Other		
Tight-fit Petri dishes	Falcon	Cat#35-1006
Glass capillary pipet	VWR	Cat#53432-706
625nm red LED	LEDsupply	Cat#CREEXPE2-RED-1
Webcam (LifeCam Studio)	Microsoft	Cat#Q2F-00013
Arduino microcontroller	Arduino Uno	Cat#A000066

LEAD CONTACT AND MATERIALS AVAILABILITY

Further information and requests for resources and reagents should be directed to and will be fulfilled by the Lead Contact, Anupama Dahanukar (anupama.dahanukar@ucr.edu). There are no restrictions on reagent sharing to disclose.

EXPERIMENTAL MODEL AND SUBJECT DETAILS

Drosophila melanogaster

Flies were reared on standard cornmeal-dextrose-agar food at 25°C and 60%–70% relative humidity under a 12 h:12 h dark:light cycle. The following fly lines were used: *Poxn*$^{\Delta M22\text{-}B5}$ (Boll and Noll, 2002), *Poxn*^{70} (Awasaki and Kimura, 1997), *Gr-GAL4* (Ling et al., 2014; Weiss et al., 2011), *Gr66a-GAL4* (BDSC#28801), *Ir-GAL4* (Koh et al., 2014), *Ir25a-GAL4* (BDSC#41728), *Ir100a-GAL4* (BDSC#41743), *Ir76b-GAL4* (BDSC#41730), *Ir94f-GAL4* (BDSC #60727), *ppk28-GAL4* (Cameron et al., 2010), *UAS-CsChrimson* (BDSC#55136), *UAS-GCaMP6s* (BDSC#42748), *trans-Tango* (Talay et al., 2017). For experiments using *Poxn* mutants, we confirmed the *Poxn* mutant background in all sorted flies by scoring the transformed long and bent mechanosensory hairs in the labellum, and three fused distal segments in the tarsi.

METHOD DETAILS

Binary Choice Feeding Assays

Feeding preference assays were performed as described previously (Charlu et al., 2013). Briefly, flies were sorted into groups of 10 males and 10 females upon eclosion and aged for 5-8 days. Since *Poxn* mutant male flies are sterile, we added 2 heterozygous males with curly wings (*Poxn/CyO*) in each group to ensure that all sorted females were mated. Heterozygous males were discarded while scoring for abdominal color. Flies were starved for 24 hr on water-saturated tissues and then placed in tight-fit Petri dishes (Falcon, #35-1006) with eighteen 10 μL dots of 0.75% agarose that alternated in tastant and color using either 25 mg/mL indigo carmine (Sigma, #I8130) or 50 mg/mL sulforhodamine B (Sigma, #230162). We used sulforhodamine B for aversive tastants and indigo carmine for the sucrose control in Figures 1A–1D. For the binary choice feeding assays in Figures 3, 6, and S1, we swapped dyes for each tastant with similar numbers of trials to account for any dye preference. We observed a strong dye preference for sulforhodamine B that resulted in a bimodal distribution of all data points in flies that lost most if not all taste sensing ability (e.g., *Poxn, Ir25a-silenced* flies in Figure 3B). Flies were allowed to feed for 2 hours at 25°C in a dark, humidified chamber, after which they were frozen and scored for abdomen color by dissecting the guts within 24 hours. Each experiment was performed between ZT 2 and ZT 8. Trials with participation lower than 50% were excluded. Preference index (PI) was calculated as ((# of flies labeled with the tastant color) – (# of flies labeled with the control color))/(total number of flies that fed). Thus, a PI of 0 would indicate an equal preference between the two choices. In all cases, PI values were calculated for mixed populations of males and females.

Activity-Recording CAFE Assay (ARC)

Total food intake, meal size, and meal frequency data were collected using the ARC as described previously (Murphy et al., 2017). Male flies were maintained on standard medium until 5-8 days old. The day before the experiment, the animals were loaded by mouth pipette into standard ARC chambers, one fly per well, and allowed to acclimate overnight with access to 5% sucrose + 5% yeast extract food in a glass capillary pipet (VWR 53432-706). Capillaries were switched the next day to those containing test diets (typically at ZT 6) and the meniscus level of each capillary was tracked for 24 hours. Drops in meniscus position above the threshold were considered feeding events, and feeding bouts less than 2 minutes apart were considered to be part of the same meal. The identity of the test diets was blinded to the experimenters throughout the assay.

Optogenetic-Activity-Recording CAFE Assay (Optogenetic-ARC)

Optogenetic stimulation of single pharyngeal GRNs in the ARC was run as described above with the following alterations. Flies were reared and maintained in darkness, and transferred to standard medium containing 400 μM all-trans retinal (ATR, Sigma, #R2500) upon eclosion. Standard ARC chambers were modified such that a red LED (625nm; LEDsupply CREEXPE2-RED-1) was placed directly behind the tip of each experimental capillary. A standard webcam (Microsoft LifeCam Studio), an Arduino microcontroller (Arduino Uno), and a custom Python script based on OpenCV were used to control the LEDs and automatically track food level at 20 Hz. The current position of each meniscus was compared to the average of its positions in the 60 preceding frames (moving average) to account for the discrete nature of pixel values and increase spatial sensitivity. A suprathreshold drop in the meniscus position, relative to the moving average, was used as a proxy indicator of food consumption for each animal. We used a threshold value of 0.0175 pixel, which was empirically determined to limit false positive rate to below 1.5%. Each detection of feeding immediately triggered the onset of the respective LED for 5 s. Thus, all consumption events elicited a minimum of 5 s of stimulation, and the duration of stimulation was directly proportional to the duration of the particular feeding event. 100 mM sucrose solution was used as the test diet for all optogenetic experiments in the ARC, and each experiment started around ZT 2 and ran for 6 hours.

Radiolabeled Food Intake Measurement

Total consumption of radiolabeled medium was measured as described previously (Deshpande et al., 2014). Briefly, mixed sex groups of flies were maintained on standard medium until the start of the experiment and the flies were 5-8 days old. Flies were transferred to vials containing [α-32P]-dCTP (PerkinElmer, Cat#NEG013H100UC) labeled diets (typically at ZT 3). After 24 hours, flies were collected in empty vials and frozen. Flies were subsequently sorted by sex for liquid scintillation counting. Total consumption was calculated using aliquots of the radiolabeled medium as a calibration.

Calcium Imaging

Calcium imaging of cell bodies in the pharynx was performed as described with some modifications (Joseph et al., 2017). Briefly, 1-week old male and female flies expressing *UAS-GCaMP6s* driven by *Gr43a-GAL4* or *Ir94f-GAL4* were starved overnight at 25°C and 60%–70% relative humidity. Mated females were then decapitated, and the labial palps of the labellum were carefully excised using a sharp razor blade to increase access to pharyngeal sensilla. Heads were mounted in a minimal volume of water on a microscope slide with three 18 × 18 mm bridging slips, placed to make two channels between the bridging slips, which allowed liquid to perfuse through the sample. A 22 × 40 mm coverslip was secured with nail polish on top of the bridging slips, positioned approximately 20 mm from the edge of microscope slide, to allow placement of tastant solution. *UAS-GCaMP6s* fluorescence was viewed with an upright Zeiss 510 confocal or an inverted Leica SP5 confocal microscope. Neurons were visualized with a 10 × objective, with a digital zoom of 4-5. Images were acquired at 512 × 512 resolution with no line averaging, with one frame scanned per second. The pinhole was calibrated to an optical slice of 100 μm, with the 488 nm laser at 25% power. Changes in fluorescent activity were recorded for 4 minutes after delivery of the stimulus. Before stimulus, focal landmarks were identified in the primary channel used to detect green fluorescent activity of the GCaMP reporter, and in a secondary channel (either DIC or a fluorescence channel outside the activation/detection range of GCaMP) used to image the pharyngeal structure during the experiment. These focal landmarks were monitored throughout the assay, to ensure that the sample remained in the correct plane of focus. If the sample shifted slightly out-of-focus along the z axis, the preparation was refocused to the reference landmarks. The out-of-focus frames were excluded from the $(\Delta F/F)_{MAX}$ calculations, depicted as gaps in representative traces (Figures S2 and S3). Fluorescence intensities were obtained with open-source Fiji/ImageJ software (https://fiji.sc). A region-of-interest (ROI) was drawn around individual cell bodies; an ROI of identical dimensions was also placed over a non-neuronal area of the image, which was used as a reference for measuring any non-specific background changes in fluorescence. Average pixel intensity for ROIs during each frame was measured with the Time-Series Analyzer Plugin, written by Balaji, J. (https://imagej.nih.gov/ij/plugins/time-series.html). A corrected average intensity for the cell body ROI was measured in each frame by subtracting the average intensity of the background ROI from the average intensity of the cell body ROI. Maximum changes in fluorescent activity were calculated as: $(\Delta F/F)_{MAX}$ = [(corrected intensity of ROI) – (average corrected intensity of 10 frames preceding stimulus)] / (average corrected intensity of 10 frames preceding stimulus). $(\Delta F/F)_{MAX}$ were then determined for either the entire 3-min sampling period or in binned 30 s intervals, following the stimulus.

trans-Tango

For tracing pharyngeal second-order taste circuits, we recombined $Poxn^{70}$ with *trans-Tango* transgenes to create $Poxn^{70}$, *trans-Tango*. Genetic crosses for tracing different pharyngeal *chemoreceptor-GAL4*-labeled GRNs in a *Poxn* mutant background were maintained at 18°C. Flies were tested when about 1-month-old, anesthetized on ice, and dissected for brain tissue in 1 × PBST (PBS with 0.3% Triton X-100). Brains were fixed for 30 min with 4% paraformaldehyde in 1 × PBST at room temperature. After three washes with 1 × PBST, samples were blocked with 5% normal goat serum (Sigma, #G9023) in 1 × PBST. Tissues were incubated in primary antibody solutions for 3 days at 4°C. Primary antibodies were: chicken anti-GFP (1:5000; Abcam, #ab13970), rabbit anti-DsRed (1:200; Clontech, #632496), and mouse anti-nc82 (1:20; Developmental Studies Hybridoma Bank). Secondary antibodies (1:400; Invitrogen) were: goat anti-chicken Alexa Fluor 488, goat anti-rabbit Alexa Fluor 568, and goat anti-mouse Alexa Fluor 647. Samples were mounted in 80% glycerol in 1 × PBST or VECTASHIELD antifade mounting medium (Vector Laboratories, #H-1000)

and stored at 4°C. Fluorescent images are acquired using a Leica SP5 confocal microscope with 400 Hz scan speed in 512 × 512 or 1024 × 1024 pixel formats. Image stacks were acquired at 1 μm optical sections. Unless otherwise noted, all images were presented as maximum projections of *z*-stacks generated using Leica LAS AF software (Leica, Microsystems GmbH).

QUANTIFICATION AND STATISTICAL ANALYSIS

Unless otherwise noted, all data are presented as median ± interquartile range. Linear regression and correlation analyses were performed using Origin 8.0 software. Statistical tests were conducted using Prism 8. For ARC data in Figures 2 and 4, the differences between means of control and *Poxn* mutant flies were evaluated with two-way ANOVA followed by post hoc Sidak's multiple comparisons test. For Ca^{2+} imaging data in Figure 5, the GCaMP6s fluorescence changes between different tastants were evaluated with Kruskal-Wallis test followed by Dunn's multiple comparisons test. To analyze the differences between transgene controls and experimental groups (planned comparisons) in Figures 3, 6, and S1, we first checked the distribution of the data with a Kolmogorov-Smirnov test for normality. If the data were not normally distributed, a Kruskall-Wallis test followed by the uncorrected Dunn's test was used. If data were normally distributed, we used parametric one-way ANOVA followed by the uncorrected Fisher's LSD test. In addition, a one sample t test (for normally distributed data) or Wilcoxon signed rank test (for not normally distributed data) was used to compare whether the preference indices in Figures 3, 6, and S1 were significantly different from 0, which represents no preference for either tastant in the binary choice feeding assays. All experiments were performed in parallel with both control and experimental genotypes. All independent trials were performed over 2 days. Complete genotypes used in this study are listed in Table S1. Complete statistical evaluations with the exact *n* for each group are listed in Table S2. The sample size for each experiment was based on previously published reports.

DATA AND CODE AVAILABILITY

All original raw data in the paper is available on Mendeley Data (http://dx.doi.org/10.17632/vj3nw2sx35.1).

Cell Reports, Volume *29*

Supplemental Information

Combinatorial Pharyngeal Taste Coding for Feeding Avoidance in Adult *Drosophila*

Yu-Chieh David Chen, Scarlet Jinhong Park, Ryan Matthew Joseph, William W. Ja, and Anupama Arun Dahanukar

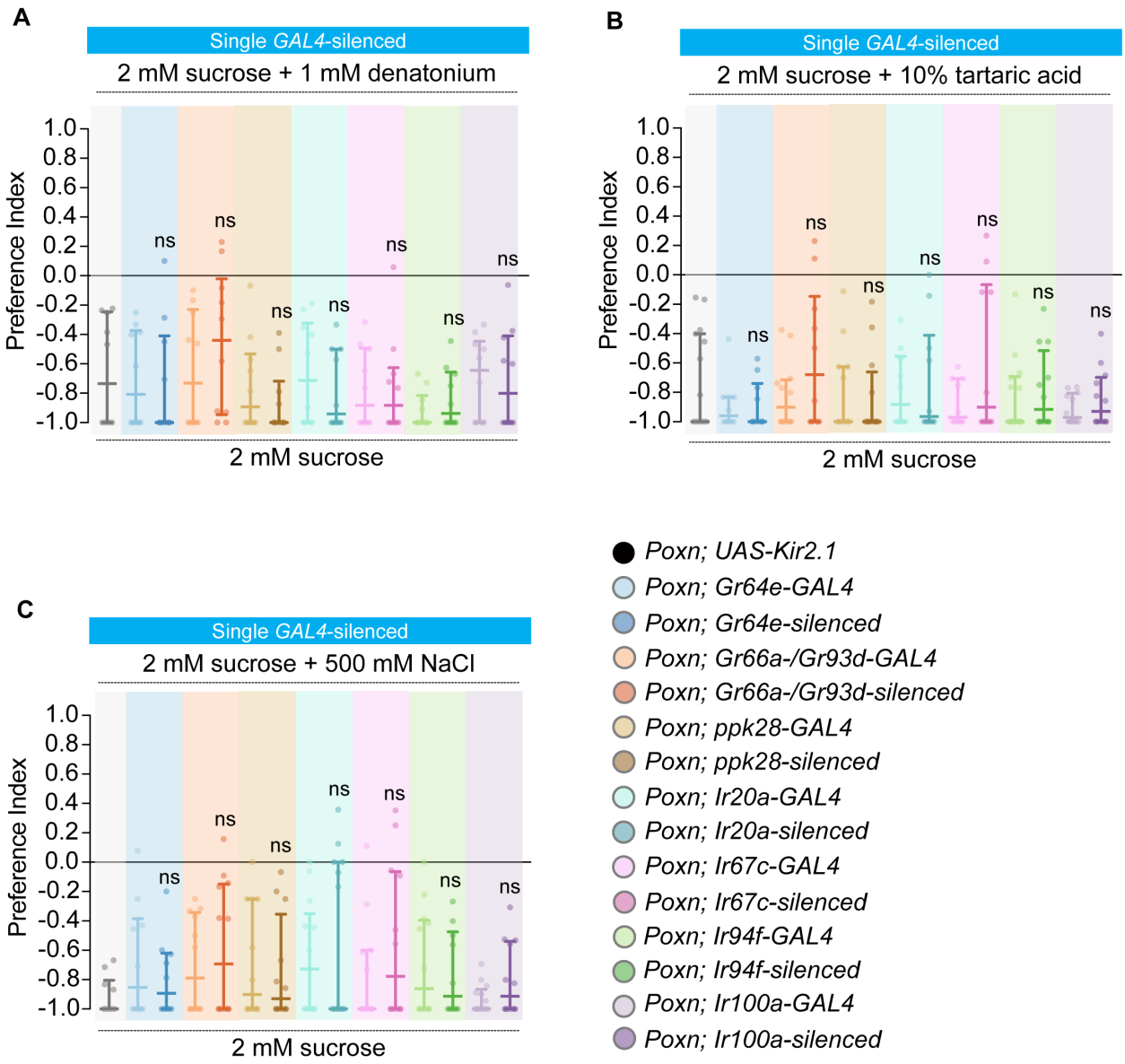

Figure S1. Multiple classes of pharyngeal GRNs are functionally redundant for driving feeding avoidance of aversive compounds. Related to Figure 3

Preference indices for sucrose/denatonium (**A**), sucrose/tartaric acid (**B**), or sucrose/high salt (**C**) mixtures tested with sucrose alone in *Poxn* ($Poxn^{\Delta M22\text{-}B5}/Poxn^{70}$) mutants carrying indicated transgenes. *UAS-Kir2.1* and *Gr/Ir-GAL4* transgenes were tested independently as indicated, or together (*Gr/Ir-silenced*). *n*=10-14. Error bars = interquartile range. ¶ and ξ indicate a statistically significant difference from the *UAS* and *GAL4* controls, respectively, by one-way ANOVA followed by uncorrected Fisher's LSD test or Kruskal-Wallis test followed by uncorrected Dunn's test. A one sample *t* test or Wilcoxon signed-rank test was used to test whether the median values for each genotype were different from zero.

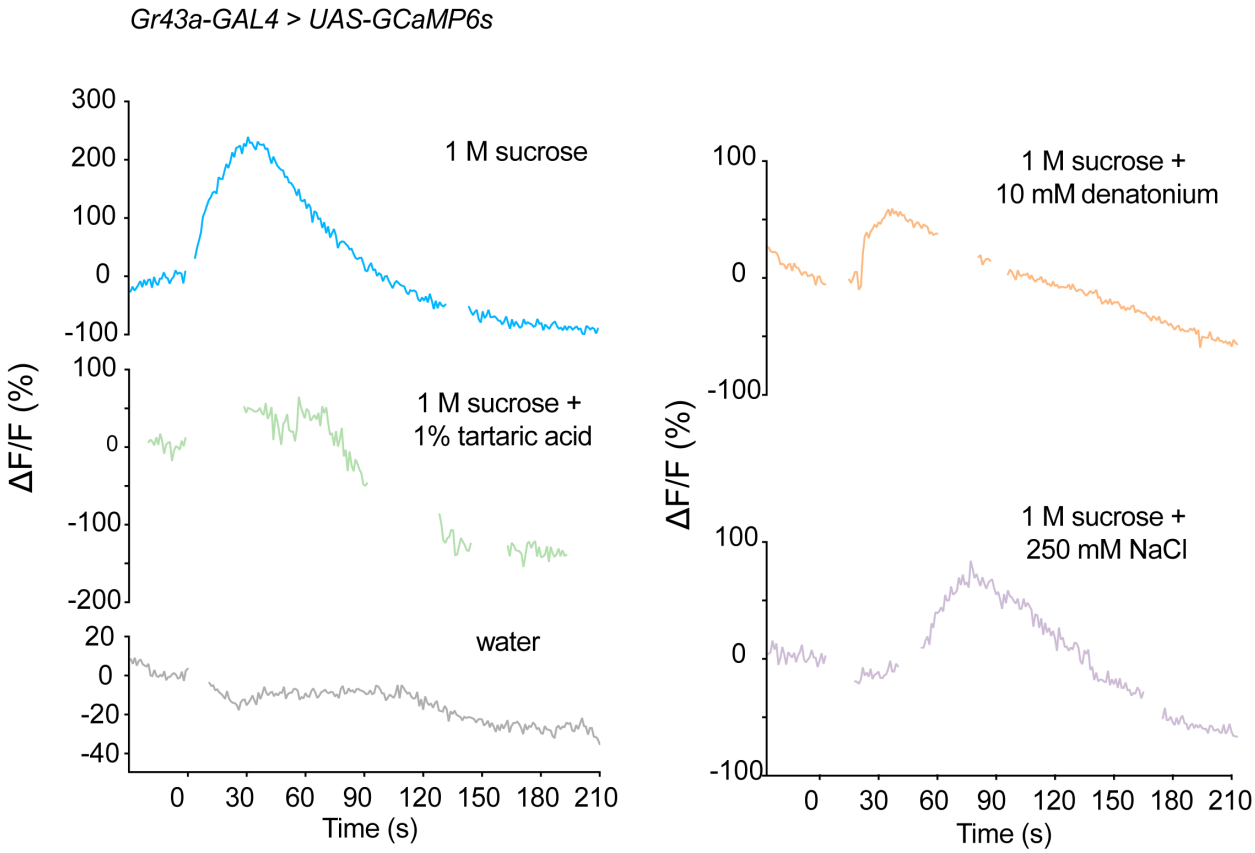

Figure S2, related to Figure 5. Representative traces of GCaMP6s fluorescence in pharyngeal *Gr43a* GRNs in response to 1 M sucrose alone or mixed with 10 mM denatonium, 1% tartaric acid, 250 mM NaCl, or water alone.

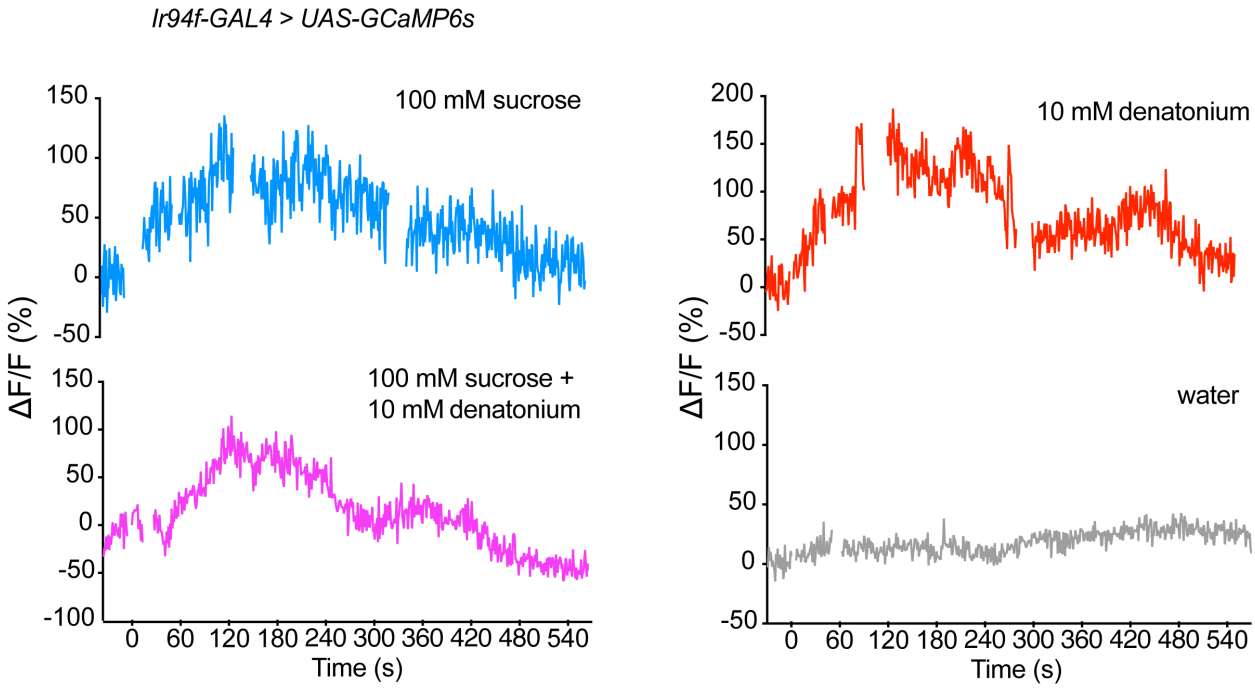

Figure S3, related to Figure 5. Representative traces of GCaMP6s fluorescence in pharyngeal *Ir60b* GRNs in response to 100 mM sucrose alone, mixture of 100 mM sucrose with 10 mM denatonium, 10 mM denatonium alone, or water alone.

Table S1. Complete genotypes of flies used in this study. Related to the STAR methods.

Figure	Genotype
1 and 2	control: *w1118*
	Poxn: $Poxn^{\Delta M22\text{-}B5}/Poxn^{70}$
3A-B	(from left to right)
	$Poxn^{\Delta M22\text{-}B5}/Poxn^{70}$; *UAS-Kir2.1/+*
	$Poxn^{\Delta M22\text{-}B5}$, *Ir25a-GAL4/*$Poxn^{70}$; *Dr or TM3/+*
	$Poxn^{\Delta M22\text{-}B5}$, *Ir25a-GAL4/*$Poxn^{70}$; *UAS-Kir2.1/UAS-Kir2.1*
3C-D	(from left to right)
	$Poxn^{\Delta M22\text{-}B5}/Poxn^{70}$; *UAS-Kir2.1/+*
	$Poxn^{\Delta M22\text{-}B5}/Poxn^{70}$; *Gr66a-GAL4/+*
	$Poxn^{\Delta M22\text{-}B5}/Poxn^{70}$; *Gr66a-GAL4/UAS-Kir2.1*
	$Poxn^{\Delta M22\text{-}B5}/Poxn^{70}$; *Gr93d-GAL4/+*
	$Poxn^{\Delta M22\text{-}B5}/Poxn^{70}$; *Gr93d-GAL4/UAS-Kir2.1*
	$Poxn^{\Delta M22\text{-}B5}$, *Gr66a-GAL4/*$Poxn^{70}$; *Gr93d-GAL4/+*
	$Poxn^{\Delta M22\text{-}B5}$, *Gr66a-GAL4/*$Poxn^{70}$; *Gr93d-GAL4/UAS-Kir2.1*
4B-C	(from left to right)
	UAS-CsChrimson/UAS-CsChrimson ; Gr23a-GAL4/Gr23a-GAL4
	UAS-CsChrimson/UAS-CsChrimson ; Gr77a-GAL4/TM3
	UAS-CsChrimson/UAS-CsChrimson ; Gr9a-GAL4/Gr9a-GAL4
	UAS-CsChrimson/UAS-CsChrimson ; +/+
5A-G	*UAS-GCaMP6s/UAS-GCaMP6s ; Gr43a-GAL4/Gr43a-GAL4*
5-H-I	*UAS-GCaMP6s/UAS-GCaMP6s ; Ir94f-GAL4/Ir94f-GAL4*
6A-C	(from left to right)
	$Poxn^{\Delta M22\text{-}B5}/Poxn^{70}$; *UAS-Kir2.1/+*
	$Poxn^{\Delta M22\text{-}B5}$, *Gr64e-GAL4/*$Poxn^{70}$; *Gr66a-GAL4/+*
	$Poxn^{\Delta M22\text{-}B5}$, *Gr64e-GAL4/*$Poxn^{70}$; *Gr66a-GAL4/UAS-Kir2.1*
	$Poxn^{\Delta M22\text{-}B5}$, *Gr64e-GAL4/*$Poxn^{70}$; *Gr93d-GAL4/+*
	$Poxn^{\Delta M22\text{-}B5}$, *Gr64e-GAL4/*$Poxn^{70}$; *Gr93d-GAL4/UAS-Kir2.1*
	$Poxn^{\Delta M22\text{-}B5}$, *Gr64e-GAL4/*$Poxn^{70}$; *ppk28-GAL4/+*
	$Poxn^{\Delta M22\text{-}B5}$, *Gr64e-GAL4/*$Poxn^{70}$; *ppk28-GAL4/UAS-Kir2.1*
	$Poxn^{\Delta M22\text{-}B5}$, *Ir20a-GAL4/*$Poxn^{70}$; *Gr64e-GAL4/+*
	$Poxn^{\Delta M22\text{-}B5}$, *Ir20a-GAL4/*$Poxn^{70}$; *Gr64e-GAL4/UAS-Kir2.1*
	$Poxn^{\Delta M22\text{-}B5}$, *Ir67c-GAL4/*$Poxn^{70}$; *Gr64e-GAL4/+*
	$Poxn^{\Delta M22\text{-}B5}$, *Ir67c-GAL4/*$Poxn^{70}$; *Gr64e-GAL4/UAS-Kir2.1*
	$Poxn^{\Delta M22\text{-}B5}$, *Gr64e-GAL4/*$Poxn^{70}$; *Ir94f-GAL4/+*
	$Poxn^{\Delta M22\text{-}B5}$, *Gr64e-GAL4/*$Poxn^{70}$; *Ir94f-GAL4/UAS-Kir2.1*
	$Poxn^{\Delta M22\text{-}B5}$, *Gr64e-GAL4/*$Poxn^{70}$; *Ir100a-GAL4/+*
	$Poxn^{\Delta M22\text{-}B5}$, *Gr64e-GAL4/*$Poxn^{70}$; *Ir100a-GAL4/UAS-Kir2.1*
	$Poxn^{\Delta M22\text{-}B5}$, *Ir76b-GAL4/*$Poxn^{70}$; *Dr or TM3/+*
	$Poxn^{\Delta M22\text{-}B5}$, *Ir76b-GAL4/*$Poxn^{70}$; *UAS-Kir2.1/UAS-Kir2.1*
7A	*UAS-myrGFP.QUAS-mtdTomato-3xHA ;* $Poxn^{70}$*, trans-Tango/Cyo ; Gr32a-GAL4/+*
7Ai	*UAS-myrGFP.QUAS-mtdTomato-3xHA ;* $Poxn^{\Delta M22\text{-}B5}/Poxn^{70}$ *, trans-Tango ; Gr32a-GAL4/+*
7Aii	*UAS-myrGFP.QUAS-mtdTomato-3xHA ;* $Poxn^{\Delta M22\text{-}B5}/Poxn^{70}$ *, trans-Tango ; Ir11a-GAL4/+*
7Aiii	*UAS-myrGFP.QUAS-mtdTomato-3xHA ; trans-Tango/+ ; Gr9a-GAL4/+*
7B	*UAS-myrGFP.QUAS-mtdTomato-3xHA ;* $Poxn^{\Delta M22\text{-}B5}/Poxn^{70}$ *, trans-Tango ; Gr61a-GAL4/+*
7Bi	*UAS-myrGFP.QUAS-mtdTomato-3xHA ;* $Poxn^{\Delta M22\text{-}B5}/Poxn^{70}$ *, trans-Tango ; Gr64c-GAL4/+*
7Bii	*UAS-myrGFP.QUAS-mtdTomato-3xHA ;* $Poxn^{\Delta M22\text{-}B5}/Poxn^{70}$ *, trans-Tango ; Gr64d-GAL4/+*
7Biii	*UAS-myrGFP.QUAS-mtdTomato-3xHA ;* $Poxn^{\Delta M22\text{-}B5}$*, Gr64e-GAL4/*$Poxn^{70}$ *, trans-Tango ; +/+*
7C	*UAS-myrGFP.QUAS-mtdTomato-3xHA ; trans-Tango/+ ; Gr23a-GAL4/+*

7Ci	*UAS-myrGFP.QUAS-mtdTomato-3xHA ; Poxn$^{\Delta M22\text{-}B5}$/Poxn^{70} , trans-Tango ; ppk28-GAL4/+*
7Cii	*UAS-myrGFP.QUAS-mtdTomato-3xHA ; Poxn$^{\Delta M22\text{-}B5}$, Ir20a-GAL4 /Poxn^{70} , trans-Tango ; Dr or TM3/+*
7Ciii	*UAS-myrGFP.QUAS-mtdTomato-3xHA ; trans-Tango/Ir67c-GAL4 ; Dr or TM3/+*
7Civ	*UAS-myrGFP.QUAS-mtdTomato-3xHA ; trans-Tango/+ ; Ir94f-GAL4/+*
7Cv	*UAS-myrGFP.QUAS-mtdTomato-3xHA ; trans-Tango/+ ; Ir100a-GAL4/+*
S1A-C	(from left to right)
	Poxn$^{\Delta M22\text{-}B5}$/Poxn^{70}; UAS-Kir2.1/+
	Poxn$^{\Delta M22\text{-}B5}$, Gr64e-GAL4/Poxn^{70}
	Poxn$^{\Delta M22\text{-}B5}$, Gr64e-GAL4/Poxn^{70}; UAS-Kir2.1/+
	Poxn$^{\Delta M22\text{-}B5}$, Gr66a-GAL4/Poxn^{70}; Gr93d-GAL4/+
	Poxn$^{\Delta M22\text{-}B5}$, Gr66a-GAL4/Poxn^{70}; Gr93d-GAL4/UAS-Kir2.1
	Poxn$^{\Delta M22\text{-}B5}$/Poxn^{70}; ppk28-GAL4/+
	Poxn$^{\Delta M22\text{-}B5}$/Poxn^{70}; ppk28-GAL4/UAS-Kir2.1
	Poxn$^{\Delta M22\text{-}B5}$, Ir20a-GAL4/Poxn^{70}; Dr or TM3/+
	Poxn$^{\Delta M22\text{-}B5}$, Ir20a-GAL4/Poxn^{70}; UAS-Kir2.1/Dr or TM3
	Poxn$^{\Delta M22\text{-}B5}$, Ir67c-GAL4/Poxn^{70}; Dr or TM3/+
	Poxn$^{\Delta M22\text{-}B5}$, Ir67c-GAL4/Poxn^{70}; UAS-Kir2.1/Dr or TM3
	Poxn$^{\Delta M22\text{-}B5}$/Poxn^{70}; Ir94f-GAL4/+
	Poxn$^{\Delta M22\text{-}B5}$/Poxn^{70}; Ir94f-GAL4/UAS-Kir2.1
	Poxn$^{\Delta M22\text{-}B5}$/Poxn^{70}; Ir100a-GAL4/+
	Poxn$^{\Delta M22\text{-}B5}$/Poxn^{70}; Ir100a-GAL4/UAS-Kir2.1
S2	*UAS-GCaMP6s/UAS-GCaMP6s ; Gr43a-GAL4/Gr43a-GAL4*
S3	*UAS-GCaMP6s/UAS-GCaMP6s ; Ir94f-GAL4/Ir94f-GAL4*